Noumea: A new multi-mission Cal/Val site for past and future altimetry missions?

Clémence Chupin[1], Valérie Ballu[1], Laurent Testut[1], Yann-Treden Tranchant[1], Jérôme Aucan[2]

[1]Littoral Environnement et Sociétés (LIENSs), UMR 7266, CNRS/La Rochelle Université, 2 rue Olympe de Gouges, 17000 La Rochelle, France : valerie.ballu@univ-lr.fr (V.B.), laurent.testut@univ-lr.fr (L.T.), yanntreden.tranchant1@univ-lr.fr (Y.-T.T.)

[2] Pacific Community Centre for Ocean Science, Nouméa, Nouvelle-Calédonie : jerome.aucan@ird.fr (J.A)

Correspondence to: Clémence Chupin (clemence.chup1@gmail.com)

Abstract. Today, monitoring the evolution of sea level in coastal areas is of importance, since almost 11% of the world's population leaves in low-lying areas. Reducing uncertainties in sea level estimates requires a better understanding of both altimetry measurements and local sea level dynamics. In New-Caledonia, the Noumea lagoon is an example of this challenge, as altimetry, coastal tide gauge, and vertical land movements from Global Navigation Satellite Systems (GNSS) do not provide consistent information. The GEOCEAN-NC 2019 field campaign addresses this issue with deployments of *in situ* instruments in the lagoon (GNSS buoy, pressure gauge, etc.), with a particular focus on the crossover of one Jason-series track and two Sentinel-3a missions tracks. In this study, we propose a method to virtually transfer the Noumea tide gauge at the altimetry crossover point, using *in situ* data from the field campaign. Following the philosophy of Cal/Val studies, we derive absolute altimeter bias time series over the entire Jason and Sentinel-3a periods. Overall, our estimated altimeter mean biases are slightly larger by 1-2 cm compared to Corsica and Bass Strait results, with inter-mission biases in line with those of Bass Strait site. Uncertainties still remain regarding the determination of our vertical datum, only constrained by the three days of the GNSS buoy deployment. With our method, we are able to re-analyse about 20 years of altimetry observations and derive a linear trend of -0.2 ± 0.1 mm/y over the bias time series. Compared to previous studies, we do not find any significant uplift in the area, which is more consistent with the observations of inland permanent GNSS stations. These results support the idea of developing Cal/Val activities in the lagoon, which is already the subject of several experiments for the scientific calibration phase of the SWOT wide-swath altimetry mission.

Short summary. Reducing uncertainties in coastal sea level trends estimates requires to better understand altimeter measurements and local sea level dynamics. Using long-term sea level time series from Noumea tide gauge (New-Caledonia) and *in situ* data collected as part of the GEOCEAN-NC campaign, this study presents a method inspired from Cal/Val studies to re-analyse about twenty years of altimetry observations and re-address the question of sea level evolution in the lagoon.

1. Introduction

Coastal regions concentrate a large part of the world's population and economic activities, with nearly 11% of the population living in low-lying areas (i.e. < 10m above mean sea level) (Haasnoot et al., 2021). Therefore, in a context of global climate change, monitoring sea level and its evolution in coastal areas is particularly needed. At this scale, it is also a scientific challenge because many processes can affect sea level locally, such as small-scale ocean processes, change in sea level pressure, presence of fresh water coming from estuaries or anthropogenic subsidence (Oppenheimer et al., 2019).

Today, altimetry satellites have provided almost 30-year records of global sea level variation around the world, with instantaneous sea surface height (SSH) at the centimetric level (i.e. with SSH uncertainties ranges from 3.5-3.7 cm depending on the mission and time span considered; Escudier et al., 2017), leading to uncertainties about Global Mean Sea Level (GMSL) trends around ±0.4 mm/y [1] (Ablain et al., 2019). When it comes to local sea level trends, Prandi et al. (2021) estimates a mean uncertainties of ±0.83 mm/y over the [1993-2019] period, with regions where the trend uncertainty exceeds the trend estimate. In both cases, these uncertainties remain higher than the requirements of the Global Climate Observing System (GCOS, 2022) of ±0.3 mm/y with a 90% confident interval. Thus, there is a great interest in improving sea level estimates and better characterising their uncertainties at both global and local scales (Cazenave et al., 2018; Legeais et al., 2018).

This involves improving both the understanding of altimeter measurements and the evaluation of the correction parameters, which is the central purpose of calibration and validation operations (hereafter named Cal/Val activities) (Fu and Haines, 2013). Varying Cal/Val methods and geographically diverse area is important to have representative estimation of altimeter biases (Bonnefond et al., 2011). At global scale, studies based on worldwide tide gauge network (e.g. Mitchum, 2000; Ablain et al., 2009) and relative multi-mission calibration through crossover and along-track comparisons led to assess global performance of altimeter and the geographically correlated errors. Local experiments are also needed to characterise the performance of measurement systems and monitor their stability over time. For that, several dedicated sites around the world are used: Harvest in the USA (Haines et al., 2020), Bass-Strait in Australia (Watson et al., 2011), Corsica in France (Bonnefond et al., 2019) and more recently Gavdos in Greece (Mertikas et al., 2018). Since the launch of the first precise altimetry mission, these operations enabled, for example, the detection of significant drift in the TOPEX/Poseidon observations (Nerem et al., 1997) or problems in algorithms and instruments (e.g. the unaccounted-for bias for Jason 1 and 2 missions describe in Willis, 2011).

To achieve the centimetric level, absolute Cal/Val involves overcoming the limits of *in situ* measurement systems, with the deployment over long periods of reliable and accurate instruments that can be linked to the same global reference frame as the satellite data. With the idea of taking advantage of the existing *in situ* systems (e.g. long-term tide gauge measurements,

---

[1] Results over period [1993-2017] with 90% confident interval

permanent GNSS sites, weather stations, etc.), the location of these sites is important. Coastal areas then seem to be an ideal compromise, but with an altimeter comparison point in the open ocean to avoid – among other things – issues related to land contamination of the altimeter and radiometer signals (Gommenginger et al., 2011). Diversifying *in situ* instrumentation is also a key factor to reduce biases related to the technique used, and multiply the comparison sites help to avoid geographically correlated errors such as those due to local site configuration (e.g. some local hydrodynamic effects) or regionally correlated altimeter errors (e.g. orbit, SSB, etc.).

This issue of better understanding altimeter measurement and local sea level dynamics was the motivation of our study in the Noumea lagoon in New Caledonia. In this area, the question of long-term sea level evolution is an unresolved issue: several studies have shown that altimetry measurements do not agree with observations from tide gauges and permanent GNSS stations (Aucan et al., 2017; Martínez-Asensio et al., 2019; Ballu et al., 2019). Following the philosophy of absolute Cal/Val studies, we therefore sought to use two major advantages of the lagoon: (1) the presence of a crossing point of three altimeter tracks from two different missions and (2) the presence of the Noumea tide gauge, which provides a long-term sea level time series. This particular configuration makes it also a relevant site to test and improve *in situ* measurements techniques in the specific environment of a lagoon: this was done during the dedicated GEOCEAN-NC cruise in October 2019. Thanks to the variety of observation collected as part of this field campaign, the present paper details a methodology to compare altimetry and *in situ* measurements. Our study site and the GEOCEAN-NC cruise and its objectives are described in Section 2. Then, Section 3 is dedicated to the processing of the *in situ* data to reconstruct a long sea level time series under the altimetry tracks. Finally, section 4 details the reprocessing of the altimeter data, and concludes with the comparison with *in situ* observations.

2. Noumea study site

2.1 The Noumea lagoon

In the Southwest Pacific, the lagoon surrounding New Caledonia (Fig. 1a) is the world largest lagoon with a surface of 24,000 square kilometres. Located in an active tectonic area on the Indo-Australian plate, occasional earthquakes inducing rapid vertical displacement could occur (Ballu et al., 2019). Contributions of non-tectonic processes (i.e. subsidence, post-glacial isostatic adjustments, etc.) to vertical displacements are estimated to be less than 1mm/y in the area (more details in Appendix A).

In the present study, we particularly focused on the southern part of the lagoon, near Noumea city (hereafter named "Noumea lagoon", Fig. 1b). With an average depth of 15-20 m, its dynamics are mainly dominated by semi-diurnal tides, with a mean tidal range varying from about 1.4 m at spring tides to 0.6 m at neap tides (Douillet, 1998). A more detailed description of the lagoon hydrodynamics is available in Appendix A.

The lagoon is also the subject of numerous geological, environmental and societal studies supported by the presence of IRD (Institut de Recherche pour le Développement) in Noumea, that offers expertise and resources to organize observation campaigns and analyses. A network of in situ measurements has been developed, which includes tide gauges and permanent GNSS stations from the BANIAN network (Fig. 1a, resp. green and blue dots). Previous studies have shown the difficulty of reconciling long-term sea level evolution estimates in this area, because altimetry, tide gauge and GNSS land-based observations do not provide consistent information (Aucan et al., 2017; Martínez-Asensio et al., 2019; Ballu et al., 2019 and Appendix A for a detailed review of these studies and existing time series). For example, over the altimetry period (1993-2013), Aucan et al. (2017a) find an uplift of +1.4 ± 0.7 mm/y from tide gauges and altimetry measurements that could not be explained by VLM from inland GNSS stations.

The lagoon is also of particular interest for altimetry : it is covered by many altimetry tracks from past and current nadir altimetry missions (TP/Jason, Sentinel-3a…) and is already the target of dedicated Cal/Val campaigns planned during the fast-sampling phase of the future SWOT[2] large-swath mission (e.g. project "SWOT in the Tropics" - Gourdeau et al., 2020). Our study focused on the notable intersection of three altimetry tracks (Fig. 1b, black lines) at about 13 km from the main land coast and 28 km from Numbo tide gauge: the TP/Jason pass #162 and Sentinel-3a passes #359 and #458.

2.2 The GEOCEAN-NC 2019 field campaign

In October 2019, the GEOCEAN-NC oceanographic cruise was organised in Noumea lagoon on the R/V Alis (Ballu, 2019) to address the question of long-term sea level evolution (see section 2.1 and Appendix A). For that, one objective was to collect *in situ* data under satellite tracks. For the 3 weeks of the campaign, a GNSS floating carpet (i.e. CalNaGeo) was towed by R/V Alis along and across altimetry tracks, and inside and outside the lagoon (Fig. 1b, blue lines). This system consists of an inflatable boat connected to a floating soft shell, on which a geodetic GNSS antenna is installed (see Chupin et al., 2020 for a detailed description). Several studies have demonstrated the capability of CalNaGeo to accurately the map sea surface in motion in various sea and weather conditions (Chupin et al., 2020; Bonnefond et al., 2022b).

---

[2] More information about the SWOT (Surface Water and Ocean Topography) mission are available on www.swot.jpl.nasa.gov
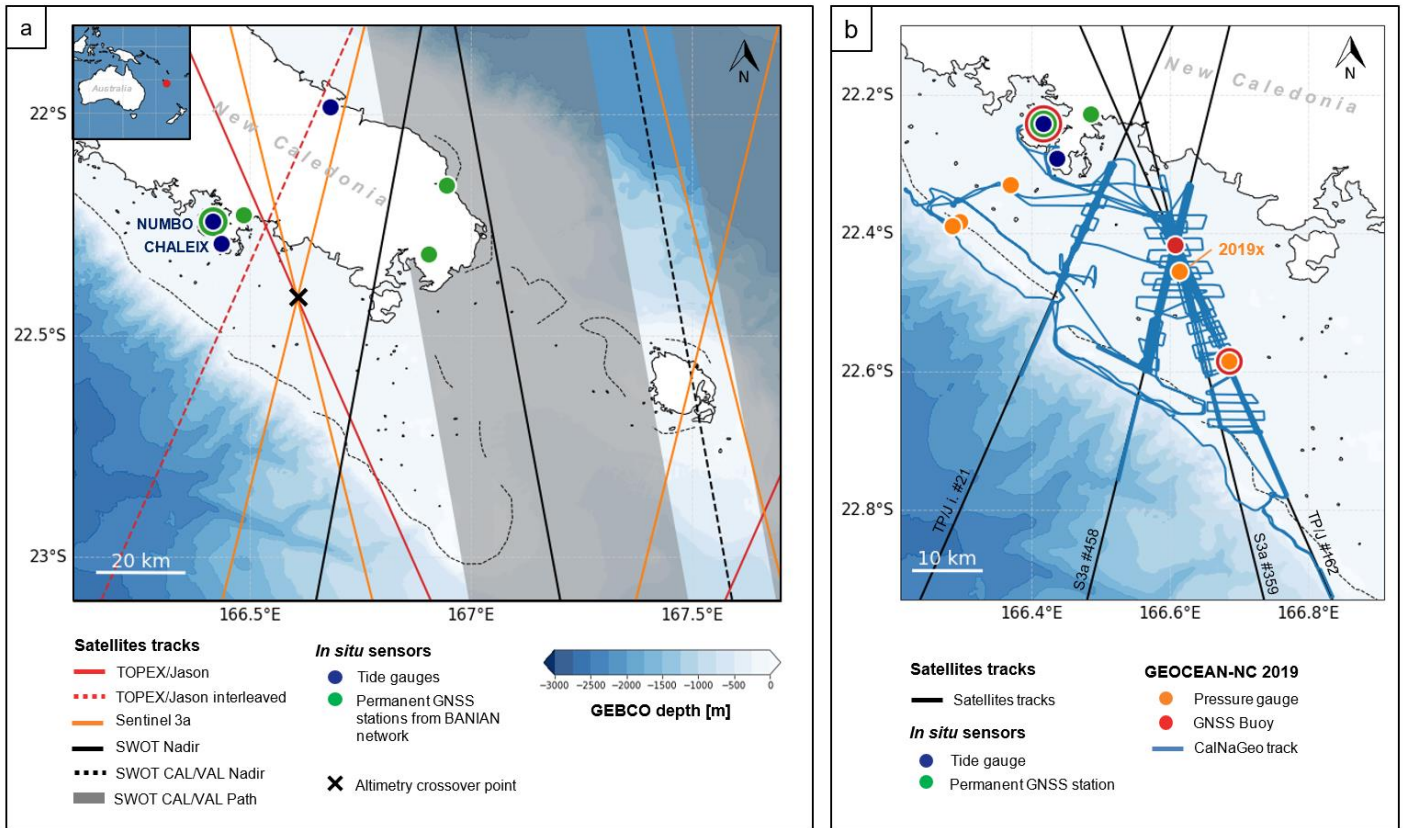
Figure 1. (a) Map of the Noumea lagoon in the South Pacific Ocean and localisation of the main altimetry tracks and *in situ* sensors. The bathymetry from the GEBCO global model (GEBCO Compilation Group 2020) is represented by a blue gradient and the dotted lines represent the coral reefs. The black cross highlights the altimetry crossover point used in this study. In-situ field campaigns will be conducted soon under the SWOT Cal/Val path. (b) Location of the sensors used (tide gauge, GNSS stations) and deployed (pressure gauge, GNSS buoy and CalNaGeo GNSS carpet) during the GEOCEAN-NC 2019 cruise. Note that some sensors were deployed at the same location: the coloured dots representing them therefore overlap.

A GNSS buoy was also successively moored at multiple locations in the lagoon (Fig. 1b, red dots), for periods of a few hours (e.g. at Numbo tide gauge) to a few days (e.g. at the crossover location). Developed by DT-INSU (*Division Technique de l'Institut National des Sciences de l'Univers*), it consists of a GNSS antenna (Trimble Zephyr 3) supported by a floating

120   structure, with a metal cylinder containing the receiver (Trimble NetR9) and batteries (see picture in Fig. 3). GNSS buoys are commonly used for Cal/Val activities (Born et al., 1994; Watson et al., 2011; Bonnefond et al., 2013; Zhou et al., 2023) and many studies have demonstrated their capability to provide sea level records with centimetric accuracy (André et al., 2013; Gobron et al., 2019). During the campaign, a calibration session was performed at the Noumea Numbo tide gauge to assess the performance of these GNSS instruments. Our results show that, despite vertical biases (−1.7 ± 0.5 cm for the buoy and -

125   0.6 ± 0.4 cm for CalNaGeo) that could result from terrestrial geodesy measurements uncertainties and GNSS processes, these two instruments are consistent with the radar gauge observations (more details in Chupin et al., 2020).

During the campaign, five pressure sensors (Seabird SBE26plus) were moored in the lagoon at depths ranging from 12 to 20 m (Fig. 1b, orange dots). All sensors recorded pressure variations at the seafloor between October 2019 and November 2020. Three of them were installed along a profile linking the Noumea tide gauge and the outside border of the coral reef, with the aim of quantifying the setup induced by wind and waves. Two other gauges were deployed along the TP/Jason altimetry track #162 for the purpose of aiding analysis of altimeter data. Before and after their deployment, a calibration phase in a hyperbaric chamber was undertaken to check the proper functioning and overall drift of the gauges (detailed results are available in Appendix B).

Taking advantage of all observations acquired as part of the GEOCEAN-NC cruise, we thus develop a method to reconstruct a long term virtual *in situ* sea level time series at the altimetry crossover point (see the black cross on Fig. 1.a).

3. Reconstruction of a long term virtual *in situ* sea level time series under the altimetry tracks

3.1 Method

The objective of our analysis is to compare the offshore altimetry measurements at the Jason/Sentinel-3a crossover with *in situ* observations. For that, two methods can be adopted (Bonnefond et al., 2011): an indirect comparison, where the *in situ* measurement is distant from the altimetry pass (typically a coastal tide gauge), and a direct comparison where *in situ* sea surface height (SSH) is directly observed at the comparison point with instrumented platforms (as in Harvest Cal/Val site) or precise GNSS buoys. Following the method of Watson et al. 2011, we developed a mixed approach using both *in situ* measurements from the GEOCEAN-NC campaign and the Noumea tide gauge records.

Figure 2 summarises the three steps of this method, that are detailed in the following sections:

Step 1. The GNSS buoy deployed at the altimetry crossover point during the GEOCEAN-NC cruise provides SSH in the same reference system as the altimetry measurements (see Section 3.2 for more details).

Step 2. To extend the comparison, we use measurements from the pressure sensor closest to the altimetry crossover (hereafter named the *2019x* pressure sensor). By computing the mean offset between the GNSS buoy and this pressure gauge over common observation periods, the 2019x pressure sensor observations are linked to a global reference frame and virtually transferred to the altimeter comparison point (see Section 3.3 for more details).

Step 3. Finally, the SSH time series from the Noumea tide gauge site is used to increase the comparison duration. Using its common year of observation with the 2019x pressure gauge, the tide gauge is virtually transferred to the crossover location by computing a tidal and datum correction (see Section 3.4 for more details).
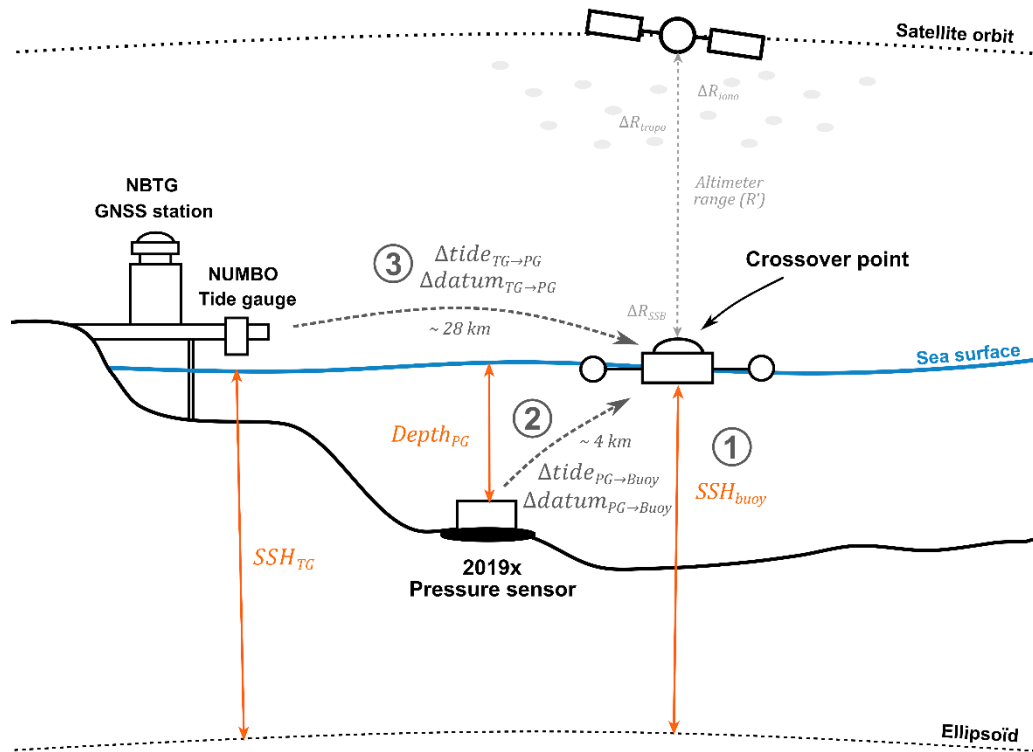
Figure 2. Configuration of the sensor's deployment. They are used to derive a long term *in situ* sea level time series under the altimetry tracks. The three steps of the methodology are represented by the circled numbers.

3.2 GNSS Buoy sea level measurements

During the campaign, a GNSS buoy was moored at multiple locations in the lagoon (see Section 2.2) and the first step of the data analysis concerns the measurement session during 3 days at the altimeter crossover point (Step 1 in Fig. 2). The processing of these data is essential as it constitutes the basis for the absolute attachment of our in-situ observations. In that sense, all errors related to GNSS processing or the application of sensor bias will directly affect the comparison with the altimeter measurements. In particular, it is important to keep in mind that during the calibration session with the Numbo tide gauge, we found a bias of 1.7cm with the tide gauge which is not yet fully understood (more details in Chupin et al., 2020).

The kinematic processing of the GNSS data was carried out with the GINS software, a scientific GNSS software (Marty et al., 2011), using the Precise Point Positioning (PPP) mode. Developed in the 90s, this method makes it possible to determine a point position without using a reference GNSS base (Zumberge et al., 1997), and recent improvements of GNSS processing

allows to compute the height of a GNSS buoy with a centimetric accuracy (Fund et al., 2013). The 10s buoy observations (i.e.

170   1 observation every 10 seconds) are processed with GINS PPP mode with the integer ambiguity resolution option (details of the processing option in Appendix C, Table C1).

The resulting sea level time series is expressed with respect to the IGSR3 reference system, that is used to make the REPRO3/MG3 orbital clock products. There is no translations/rotations vs ITRF2014, only a time-dependant vertical scale

175   and that could be approximate with : $+7.9 + 0.19\,(t - 2010)$ mm. The distance from the GNSS Antenna Reference Point (ARP) to sea level was determined using buoy dimensions and ruler readings during static sessions in Nouméa harbour. By subtracting all these corrections from the initial time series, we obtain the water level relative to the IAG-GRS80 ellipsoid. After a first data selection to keep positions determined with more than 10 satellites and remove outliers, the resulting heights are filtered using a Vondrak filter with a 30 min cut-off frequency (Vondrak, 1977) (Fig. 3). This filtering lead to a SSH time series cleaned

180   from high frequency signal (short waves, …) (Step 1 in Fig. 2), adequate for a comparison with a 20 m depth bottom pressure records (Step 2 in Fig. 2).

During the buoy deployment, the area was overflown by the Sentinel-3a satellite on its track #359, which allows a direct comparison with the buoy measurements. At the time of the overfly, the SSH difference between the filtered buoy time series

185   and altimetry measurements is about 1.4 cm (Fig. 3). As this single comparison remains limited we then use the 1-year pressure sensor observations to extend the time series of *in situ* measurements.

Buoy deployment at the crossover
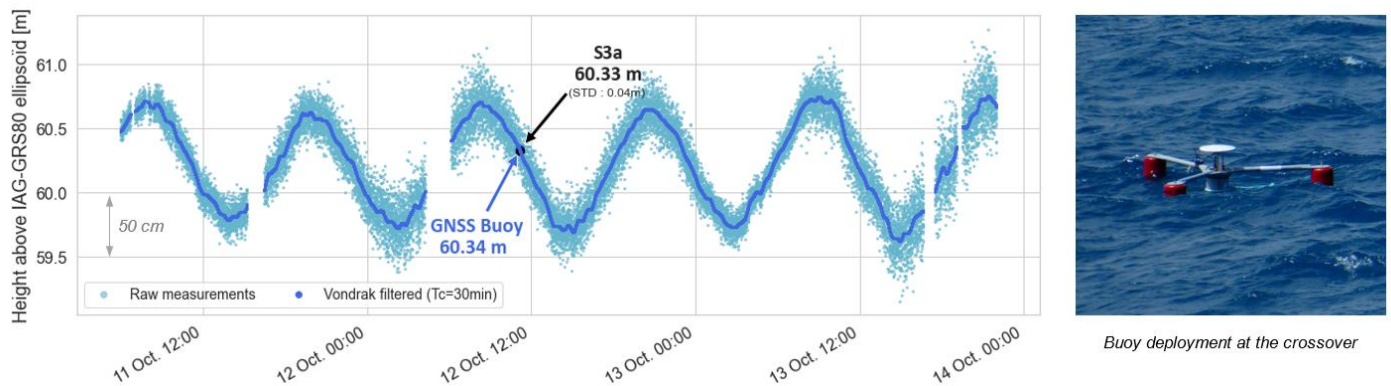
Figure 3. GNSS Buoy raw (light blue) and Vondrak filtered (dark blue) sea level heights above the IAG-GRS80 ellipsoid.

3.3 Pressure sensor observations

To extend the comparison, we used the 1-year length pressure gauge 2019x time series. The pressure gauge deployment site, located about 4 km south of the Sentinel-3a and Jason-series cross over (Fig. 1b, orange dot), was chosen as a compromise

190   between distance to the tracks intersection and the depth limitation of the SBE26plus (20 m). An analysis of the Significant

Wave Height (SWH) from both sensors shows that, despite the distance, they roughly monitor the same sea state (details of this analysis are shown in Appendix D). Thanks to the SCHISM hydrodynamic model output (Zhang et al., 2016), we also highlight a remaining tidal gradient between the two sensors that could reach ± 1cm in amplitude (see Appendix D for more details). When looking at the centimetric level, this must be considered: in the following, we then apply this tidal gradient to the pressure gauge observations to be in line with the crossover tidal regime.

We then used the GNSS buoy observations to tie the pressure gauge measurements into the same reference frame as the altimetry data (Step 2 in Fig. 2). The 2019x seafloor pressure is converted to equivalent hydrostatic heights, using atmospheric pressure time series from ERA5, the latest climate reanalysis produced by ECMWF (Hersbach et al., 2018), at the pressure gauge location, and the water column density computed with the pressure gauge temperature and a mean salinity value of 35.5 psu. The calibration phase of the 2019x sensor shows a linear trend of about -70 mm/year (more details in Appendix B), which is removed to obtain the final sea level time series from the 2019x pressure sensor.
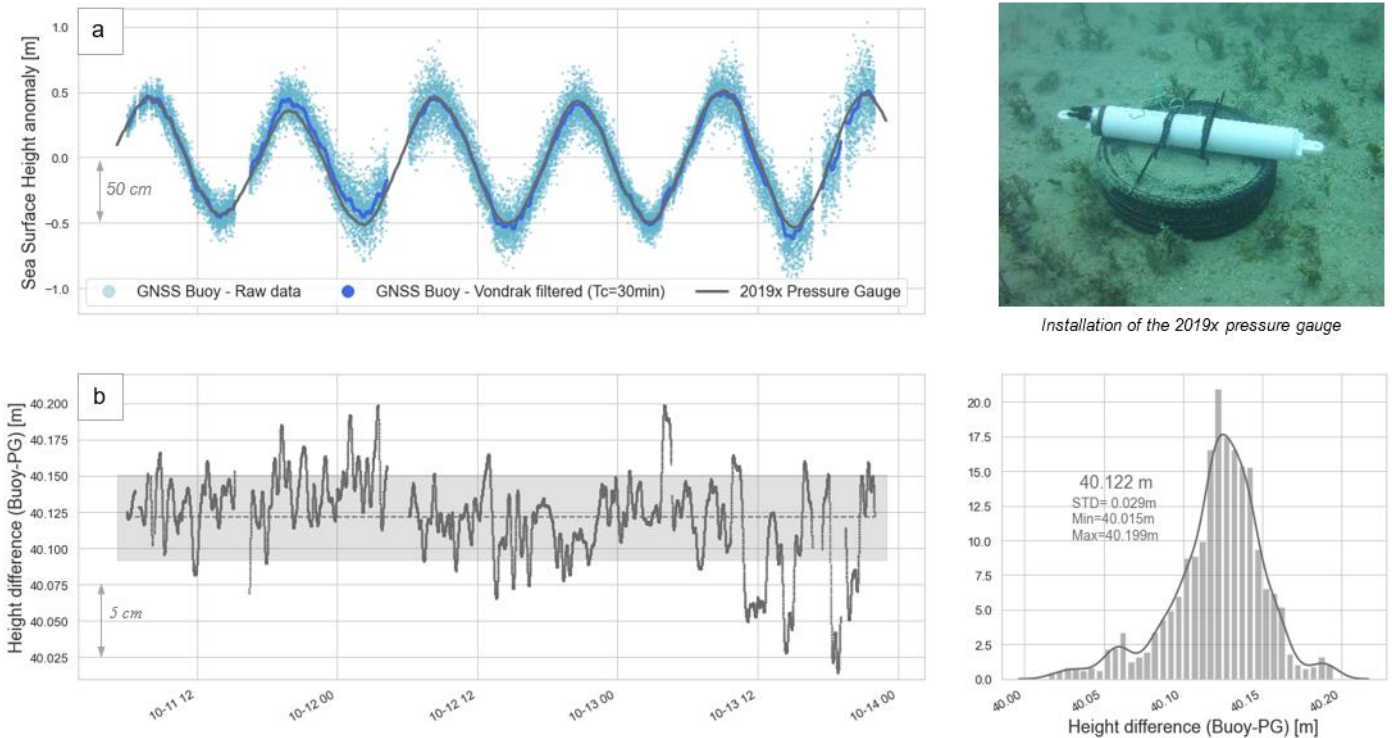
Figure 4. Comparison between GNSS buoy and 2019x pressure gauge observations / (a) Sea surface height anomaly from GNSS buoy raw data (light blue), GNSS buoy filtered data (dark blue) and 2019x pressure sensor (grey) / (b) Difference between filtered GNSS buoy and 2019x pressure gauge heights. The grey dotted line represents the mean difference (40.122 m), and the grey area represents the ± 1 standard deviation (3 cm). These differences are also showed on the lower right histogram.

The pressure gauge data are then tie to the ellipsoid by differencing the filtered GNSS buoy heights (Fig. 4a, dark blue) from the pressure sensor measurements (Fig. 4a, grey line). Over the 64 h of common observation period, the average difference is equal to 40.122 m (STD = 0.029 m - Fig. 3b). Added to the hydrostatic heights of the pressure sensor, this offset allows us to obtain a 1-year sea level record at the intersection of the altimeter tracks, thereafter named SSH_{PG} (Step 2 in Fig. 2). However, to have a longer *in situ* time series, we also considered the Noumea tide gauge dataset (Step 3 in Fig. 2).

3.4 Noumea tide gauge long term measurements

The French Hydrographic Service (Shom) provides sea level observations at Noumea through the Chaleix (operating from 1957-2005) and Numbo (2005 to present) tide gauges (Fig. 1a, blue dots). Before 1967, measurements were paper records, and electronic observations began in 1967. Thanks to a 6 months overlap of data collection, the old Chaleix site has been linked to the new Numbo site, located about 6 km away (Fig. 1a, blue dots). Aucan et al., 2017 were thus able to reconstruct the whole time series by concatenating data from 1957 to 2018, making it one of the longest series available in the South Pacific. In this paper, we used the data available online (http://uhslc.soest.hawaii.edu/data/ - ID 019) and regularly updated with the latest measurements from Numbo tide gauge. This 1-hour sampling sea level time series will be referred to as SSH_{TG} in the following, and covers the entire altimetry period and our study ([1967-2021]).

The Noumea tide gauge site and the altimeter crossover point are separated by about 28 km. The last step of our methodology is to bring tide gauge observations at the comparison point (Step 3 in Fig.2). For that, we consider the height residuals between 2019x pressure sensor and Noumea tide gauge measurements and compute a tidal and datum correction, as made by Watson et al. (2011) at the Bass Strait Cal/Val site. After linearly interpolating the 10 min pressure gauge data on the 1-hour tide gauge time series over their common measurement period (Fig. 5a), we compute the difference $[SSH_{PG} - SSH_{TG}]$ (Fig. 5b – black). We then computed an harmonic analysis on these residuals to get the tidal gradient correction in amplitude and phase ($\Delta tide_{TG \rightarrow PG}$) and the datum correction ($\Delta datum_{TG \rightarrow PG}$) to apply on the tide gauge record. Tidal residuals are mainly due to semi-diurnal waves, with a contribution from M2, S2 and N2 of about 4.5 cm, 1.7 cm and 1.1 cm respectively. The resulting datum correction is estimated to be -57.1 cm, which is coherent at the order of a few centimetres with gradients from two global gravity field models in the area (see Table F1 in Appendix F). After applying the tidal gradient and the datum offset, the difference $[SSH_{PG} - SSH_{TG}]$ have a Root-Mean-Square Error (RMSE) of 1.3 cm (Fig. 5b – grey), to compare with the 3.7 cm without these corrections.

Finally, we obtain an hourly *in situ* sea level time series at the altimeter comparison point (thereafter named $SSH_{in-situ}$) by virtually transferring the Noumea tide gauge observations (Step 3 in Fig.2) :

$$SSH_{in-situ} = SSH_{TG} + \Delta tide_{TG \rightarrow PG} + \Delta datum_{TG \rightarrow PG} \qquad (1)$$

However, the altimeter fly over the area is for about 10 seconds between 1 and 3 times per month (resp. for Sentinel-3a and Jason missions). Doing a simple linear interpolation of the hourly $SSH_{in-situ}$ at the satellite overfly time (t_{sat}) does not well reproduce the tide evolution. Thanks to a harmonic analysis over the tide gauge time series, we expressed the SSH_{TG} as a tide reconstruction at the time of the satellite flyby (hereafter named $TGtide_{rec}(t_{sat})$) and add tide residuals linearly interpolated at the flyby time (i.e. $TGtide_{res}(t_{sat})$). Thus, for the final comparison with altimetry data, the $SSH_{in-situ}$ from Eq. (1) could be explained as:

$$SSH_{in-situ}(t_{sat}) = TGtide_{rec}(t_{sat}) + TGtide_{res}(t_{sat}) + \Delta tide_{TG \to PG}(t_{sat}) + \Delta datum_{TG \to PG} \qquad (2)$$

With this method, there are still inaccuracies in the determination of the sea level due to weather and local conditions, but the tide evolution is well considered.
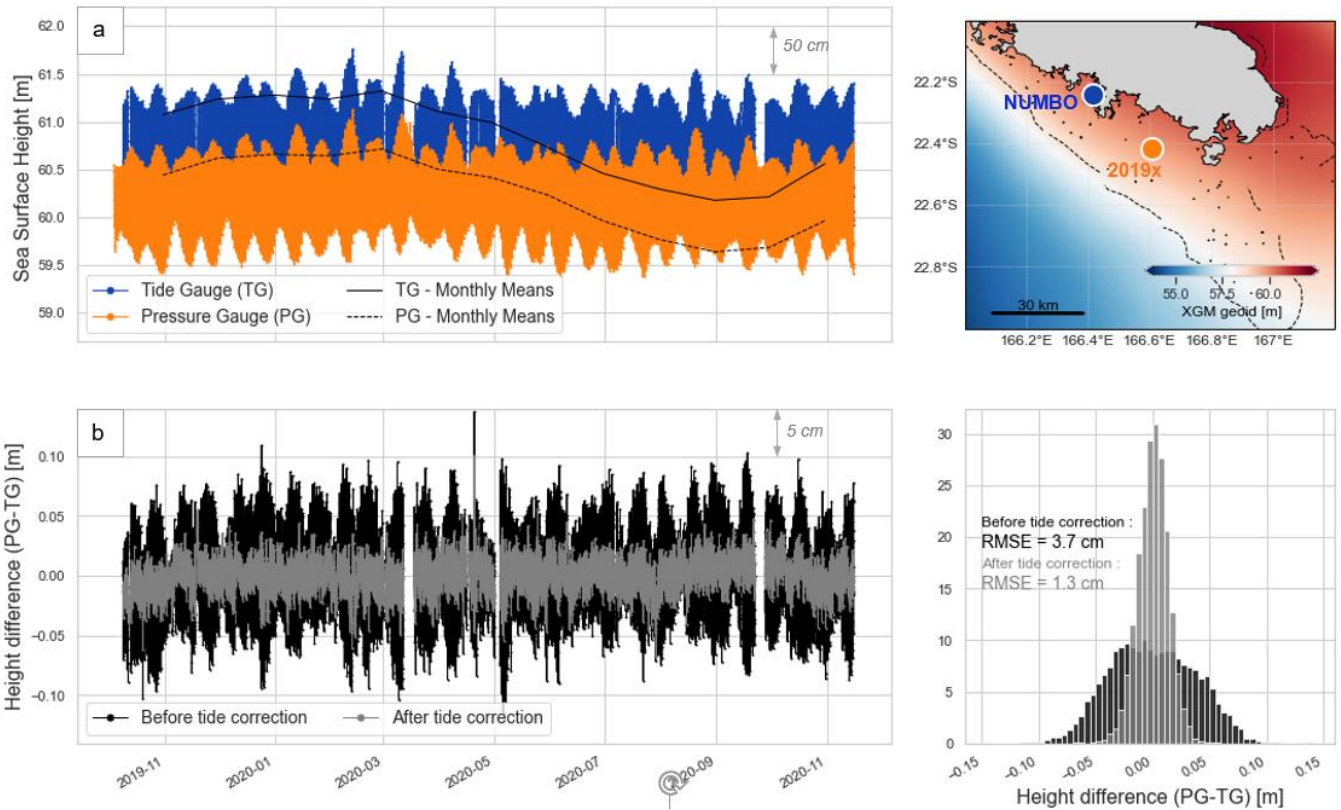
Figure 5. Tidal difference between the Noumea tide gauge (TG) and the 2019x pressure gauge (PG) / (a) Sea level record at 2019x pressure gauge (orange) and Numbo tide gauge (blue) during the common observation period (13 months). Monthly means are displayed in black (solid line for tide gauge, dotted line for pressure gauge). The two sensors are separated by about 28km. / (b) Height difference between PG and TG before (black) and after (grey) applying the tidal correction. These differences are also displayed on the histogram, with Root Mean Square Error (RMSE) values for both solutions.

4. Calibration/Validation of altimetry measurements

4.1 Altimetry data processing

4.1.1 Jason and Sentinel-3a Geophysical Data Records (GDR)

250 There is a wide variety of altimetry products and sources, allowing both advanced analysis of raw altimeter data and corrections, and access to sea level databases that can be used directly without further processing. As our study focused on the absolute bias of the altimeter SSH, we thus consider the official latest release of along-track products to derive altimeter sea level with the up-to-date instrumental and geophysical corrections parameters.

255 For the Jason track #162, we use the last Geophysical Data Records (GDR) delivered by AVISO+, that integrate precise orbits and up-to-date corrections for 20 Hz measurements (Table 1). For Sentinel-3a, we consider the SRAL Level 2 Marine data to ensure global coverage of the lagoon. These data are disseminated by EUMETSAT, the European Organisation for the Exploitation of Meteorological Satellites, previously on their CODA portal (Copernicus Online Data Access, until September 2022) and now on their Data Store (https://data.eumetsat.int). From 2016 to 2019, the Sentinel-3a data were reprocessed using

260 the current standards of the Baseline Collection 004, used for Sentinel-3a products after 2019 (Table 1).

Table 1. Altimeter products used in the study

Mission	Jason			Sentinel-3a	
	Jason 1	Jason 2	Jason 3		
Cycles	1-259	1-303	1 - 219	3-52	53-81
Products	GDR-E	GDR-D	GDR-F	SR_2_WAT Baseline Collection 004	
				Reprocessed BP 2.61	Non-reprocessed BP 2.61/2.68
Source	AVISO+ FTP : https://www.aviso.altimetry.fr/en/home.html			EUMETSAT CODA : https://coda.eumetsat.int/#/home CODA REP : https://codarep.eumetsat.int/#/home	

4.1.2 Altimetric corrections considered in order to accurately estimate sea surface height

During its propagation, the radar signal is delayed by multiple phenomena that must be consider to estimate the altimetric sea

265 surface height (SSH_{alt}) with a centimetric accuracy. Thus, the altimeter range must be corrected for instrumental errors (R'), sea state bias (ΔR_{SSB}) and atmospheric delays (ΔR_{iono} and ΔR_{tropo}). For the comparison with tide gauge measurements, it is also necessary to integrate geophysical corrections (ΔR_{geo}) to account for the effect of ocean tide loading, pole and solid earth tides.

270 In coastal areas, several factors can affect the quality of altimeter measurements. The proximity to the land can impact the echo received by the altimeter, which requires adapting the waveform retracking method (Gommenginger et al., 2011). The high variability of coastal processes, both in time and space, also limits the quality of atmospheric and geophysical corrections (Andersen and Scharroo, 2011). As this study is an opportunity to test different corrections in our area, we use GDR along-track products to select the most appropriate parameters or replace them by external products. In these files, the range is already

275 corrected from instrumental errors (R'). For our study, we also consider the ΔR_{SSB} and the ΔR_{geo} parameters at 1 Hz, linearly interpolated at the time of each 20 Hz observations (see Table 2 for a summary).

Regarding the ionospheric delay (ΔR_{iono}), GDR files provide a correction based on observations from the dual frequency altimeter (*Jason-3 Products Handbook*, 2020) that could be very noisy. To improve this correction without degrading the

280 altimeter measurements, one way is to smooth this ionospheric delay over a 150 km profile (Imel, 1994). Following methods developed on other historical Cal/Val sites (e.g. Watson et al., 2011), we use the mean ionospheric delay in the area between -23.85° and -22.5°, which covers part of the lagoon, the reef and the open ocean, and roughly corresponds to the recommended distance of 150 km.

285 The tropospheric delay (ΔR_{tropo}) can be divided into a wet and a dry component. About 90% of this delay is related to the dry component, that can be estimated with atmospheric models (Chelton et al., 2001). We use the 1 Hz hydrostatic tropospheric correction provided in the GDR files, linearly interpolated to the time of the 20 Hz measurements. The wet component of the troposphere is related to the water vapor content in the atmosphere, that could be particularly variable in time and space when approaching the coast. Onboard radiometers can estimate these variations along the track. However, radiometer footprint is

290 larger than the altimeter one (resp. ~20/30 km for the radiometer, and ~4/10 km for the altimeter): when approaching the coast, the radiometer is thus contaminated by land earlier than the altimeter measurements (Andersen and Scharroo, 2011). In the lagoon, the effect of the land contamination is visible when approaching the main island, but at our comparison point, the radiometer correction seems to be exploitable for both Jason and Sentinel-3a missions (more details in Appendix E). To confirm this hypothesis, we also test two other datasets: (1) a wet tropospheric delay provided by the European Center for

295 Medium Range Weather Forecasting (ECMWF) and (2) a wet tropospheric correction computed from inland permanent GNSS stations (more details about this processing in Appendix E). When comparing with the *in situ* observations, we will be able to analyse the impact of these different solutions (see Section 4.2.1).

Finally, altimetry satellites do not fly over the exact same point at each pass: it is therefore necessary to consider the height

300 difference between the comparison point and the actual pass of the satellite track, which we approximate to be the geoid height difference ($\Delta R_{geoïd}$). Using CalNaGeo observations during the GEOCEAN-NC campaign (Fig. 1b, blue lines), we demonstrate that the geoid gradients from the XGM 2019e gravity field model are the most suitable in our area (details are available in

Appendix E). At each pass, we therefore use this model to determine the geoid gradient to be applied. However, in the GDR, the *geoïd* variable integrates the permanent component of the solid earth tide ($\Delta R_{set_{perm}}$), while the cyclic component

305 ($\Delta R_{set_{cycl}}$) is including in the *solid_earth_tide* variable (see *Jason-3 Products Handbook*, 2020 and *IERS Convention*, 2010 for more details about this geophysical component). In our area, this permanent component reaches 3.2cm and must be corrected in the altimeter processing for a suitable comparison with the in-situ measurements.

In the end, the altimetric sea level time series at our comparison point is given by:

310
$$SSH_{alt} = H - R' - \Delta R_{iono} - \Delta R_{tropo} - \Delta R_{SSB} - \Delta R_{geo} + (\Delta R_{geoïd} - \Delta R_{set_{perm}}) \tag{3}$$

The corrections used to derive the SSH_{alt} are summarised in Table 2.

Table 2. Altimetric corrections used to derive the SSH

Parameter		Correction used
Ionosphere (ΔR_{iono})		GDR Ionospheric mean delay between [-23.85°; -22.5°]
Troposphere (ΔR_{tropo})	Dry	1Hz GDR correction linearly interpolated at the 20 Hz measurements
	Wet	Radiometer / ECMWF model / GNSS Corrections linearly interpolated at the 20 Hz measurements
Sea State Bias (ΔR_{SSB})		1Hz GDR correction linearly interpolated at the 20 Hz measurements
Geophysical (ΔR_{geo})	Ocean tide loading	
	Solid earth tide (Cyclic component - $\Delta R_{set_{cycl}}$)	
	Pole tide	
Geoïd	Gradient ($\Delta R_{geoïd}$)	XGM 2019e gravity field model (Zingerle et al., 2020)
	Solid earth tide (Permanent component - $\Delta R_{set_{perm}}$)	Computed from equations from *IERS Convention* (2010)

315

4.2 Altimetric bias computation

The determination of the altimeter bias ($\Delta Bias_{alt}$) consists of comparing the satellite observations (SSH_{alt} from Eq. (3)) with the *in situ* measurements ($SSH_{in\ situ}$ from Eq. (1)) at the time of the overfly (Bonnefond et al., 2011) :

$$Bias_{alt} = SSH_{alt} - SSH_{in\ situ} \tag{4}$$

320

At each pass, we therefore subtracted the $SSH_{in\ situ}$ from 20 Hz SSH_{alt}. All measurements within ± 1 km (about ± 0.17 s) from our comparison point are averaged to obtain a mean bias and an indicator of the altimeter bias dispersion. This method

does not follow the standard approach used in Cal/Val sites, which consists in interpolating all corrections at the Point of Closest Approach (PCA) (Bonnefond et al., 2011; Watson et al., 2011). However, our method allows us to reject cycles where the standard deviation of the mean bias is greater than 10 cm. In the GDRs, we have also collected the range MQE parameter. In the altimetry process, the *retracking* step allows to determine the range by fitting a theorical model on the radar echo recorded by the altimeter. We thus have access to a metric to assess the quality of the radar echo *retracking* result: the closer the MQE is to zero, the better the chosen model reproduce the measured waveform. With our methodology, we thus have access to the mean MQE value over the ± 1km around the comparison point. After analysing MQE values on along-track data (more details in Appendix G), we decide to remove cycles where the MQE average exceeds the threshold value of 0.01. Finally, we apply a basic outlier detection algorithm based on the interquartile range method on the bias time series.

4.2.1 Impact of the wet tropospheric correction

To determine the most appropriate solution for the wet tropospheric correction, we compute variants of the altimeter absolute bias for the Jason 3 track #162 and the 2 Sentinel-3a tracks over the [2016-2021] period, only changing the wet tropospheric parameter (see section 4.1.2 for more details). Figure 6 represents the altimetric bias at the comparison point by using the wet tropospheric correction from the radiometer (black), the ECMWF model (grey) and the GNSS based solution (coloured). It is important to note that the GNSS correction is not available for all cycles, unlike the radiometer and model ones that are directly taken from the GDR files.

For all missions, the resulting mean bias estimates could vary at the centimetric level depending the correction used, and the GNSS-based corrections seems to slightly decrease the value of the mean altimeter bias. The radiometer and the model agree well for Jason 3 mission (mean difference of 0.3 cm), whereas for the S3-a track #359, the radiometer seems closer to the GNSS estimates (mean difference of 0.4 cm). For both Jason and Sentinel-3a missions, none of these three corrections significantly improves the mean bias dispersion. When analysing the along track values of the three wet tropospheric corrections (see Appendix E), we can see that they all can be very variable according to the cycles.

In any case, there is no evidence that the radiometer correction may be wrong within our study area. These results confirm that the latest improvements in radiometer corrections now included in the GDR files can be used to derive a consistent altimeter bias. A similar conclusion was made by Bonnefond et al. (2019) at the Corsica historical Cal/Val site for Jason missions. Since GNSS data are not available for all cycles, we chose to keep the wet tropospheric radiometer correction in the following analyses.

4.2.2 Evaluation of the *in situ* SSH determination method

To evaluate our methodology for the $SSH_{in\ situ}$ reconstruction, we compared the mean bias estimated using the 2019x pressure sensor measurements with the one computed using our method (i.e. Eq. 1) over their common observation period (from October 2019 to November 2020). Figure 7 shows the evolution of the altimeter bias for the Jason and Sentinel tracks according to the *in situ* data considered. For the 3 tracks, the difference between the mean biases is a few millimetres (respectively +1/+2/+5 mm for the tracks #162/#359/#458). However, we could observe centimetre level variations in the time series of differences (lower right panels, coloured curve). Despite the use of tidal gradients to integrate differences due to hydrodynamic effects in the lagoon, some variability may still exist between the location of the tide gauge and the pressure sensor. Although it is important to take this effect into account for long-term comparisons, we can still assume that the use of the tide gauge series does not affect the estimate of the mean altimeter bias. Our tide gauge data transfer method seems to be relevant for estimating the altimeter bias at the cm-level.

Figure 6. Altimetric bias at the comparison point according to different wet tropospheric models and for 3 altimetric tracks: the Jason 3 (orange) track #162, the Sentinel-3a tracks #458 (dark blue) and #359 (light blue) / (a) Altimetric biases distribution as a function of the wet tropospheric delay from the radiometer (black), the ECMWF model (grey) and the GNSS stations (coloured). / (b) Bias time differences from the radiometer solution with respect to the ECMWF model (grey) and GNSS stations (coloured).
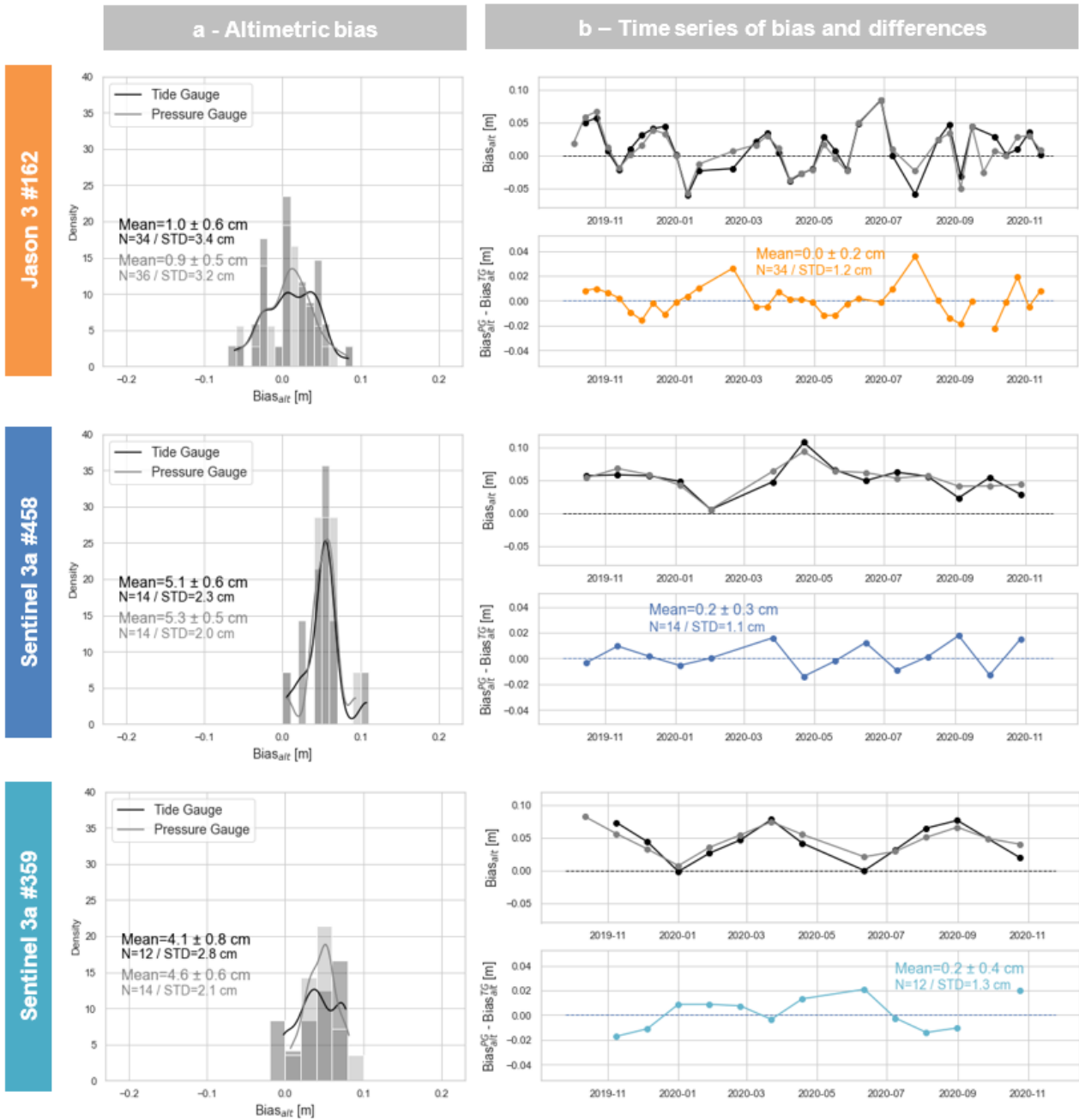
Figure 7. Altimetric bias at the comparison point according to different *in situ* datasets and for 3 altimetric tracks: the Jason 3 (orange) track #162, the Sentinel-3a tracks #458 (dark blue) and #359 (light blue). / (a) Altimetric biases distribution using tide gauge data (black) or 2019x pressure gauge (grey) as *in situ* reference. / (b) Bias time series using tide gauge (black) or pressure gauge (grey) as *in situ* dataset (upper panel) and bias time differences from the pressure sensor (lower panel).

4.2.3 Multi-mission comparison

Over period [2016-2022], both Jason 3 and Sentinel-3a are measuring sea level at our crossover point, that allow a direct inter-
370 mission comparison. Figure 8 shows the altimetric biases time series for Jason 3 (mean bias of +12 ± 3 mm, orange line) and
Sentinel-3a tracks #359 (+40 ± 4 mm, light blue line) and #458 (+39 ± 3 mm, dark blue line) at our comparison point. Table 3
summarises the last results of the three historical Cal/Val sites from the last Ocean Surface Topography Science Team (OSTST)
meeting (Bonnefond et al., 2022a). For Jason 3, our mean bias estimate is close to the Harvest one (-2 mm), and slightly higher
than the Corsica (+8 mm) and Bass-Strait results (+16 mm). For Sentinel-3a, we find a mean bias larger of about +16 mm
375 compared to the Corsica and Bass Strait sites. Regarding the inter-mission bias $[Bias_{alt}^{S3a} - Bias_{alt}^{J3}]$, we find a difference of
+28 mm, which is in line with those determined at Bass-Strait (+29 mm) and Corsica (+18 mm) sites (see Table 3).

The consistency of these results suggests that our methodology is suitable for estimating absolute biases. However, one must
remember that it may remain uncertainties in the determination of the $SSH_{in\ situ}$. In this study, the absolute referencing of the
380 *in situ* data is based on the 3 days of the GNSS buoy mooring, and many factors can influence these results at the centimetric
level. These include the choice of the GNSS processing parameters, inaccuracies related to the integration of sensors biases or
reference system changes, and the effect of the tether tension on the buoyancy as demonstrated at Bass Strait site (Zhou et al.,
2020). One need to remember that during the buoy calibration session, we found a bias of 1.7cm with the tide gauge which is
not yet fully understood (Chupin et al., 2020). Besides, although we show that our tide gauge data transfer method is relevant
385 (see Section 4.2.2), there may remain some unaccounted-for dynamic processes between the tide gauge and the comparison
point that may lead to inaccuracies. To consolidate the vertical datum, new geodesy measurements with a good calibration
session should be conducted to reduce uncertainties in the $SSH_{in\ situ}$ estimation and better constrain the altimeter biases.
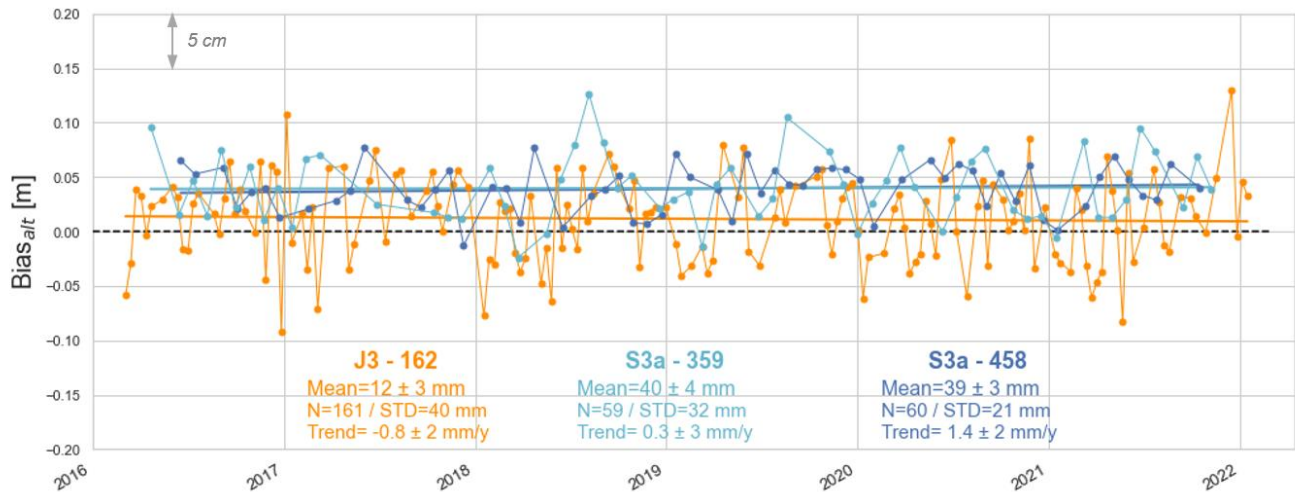
Figure 8. Altimeter bias time series at the comparison point for Jason 3 track #162 (orange) and Sentinel-3a tracks #458 (dark blue) and #359 (light blue) during their common flying period.

4.2.4 Long-term altimetric bias evolution

Thanks to the long-term measurements of the Noumea tide gauge, we compute the Jason altimeter bias time series between
390 2002 and 2022. The absolute bias estimates are detailed in Figure 9a for Jason 1 (with a mean bias of +66 ± 2 mm), Jason 2
(+39 ± 3 mm) and Jason 3 (+12 ± 3 mm). The Jason 1 and Jason 2 mean biases are slightly higher than in other Cal/Val studies
(Table 3), with a mean difference of about +24mm (J1) and +23mm (J2) compared to Corsica and Bass Strait sites. Regarding
the inter-mission biases, we find -27 mm for $[Bias_{alt}^{J2} - Bias_{alt}^{J1}]$ that is consistent with the Bass Strait estimate. For $[Bias_{alt}^{J3} -$
$Bias_{alt}^{J2}]$, we find inter-mission bias of -27 mm to compare with the -19mm and -12mm of Bass Strait and Corsica sites. These
395 results are very encouraging and show the interest of the Noumea site to conduct further Cal/Val activities. As discussed
previously, a more robust referencing of the *in situ* data could lead to the determination of better constrained biases.

To the first order, the altimeter bias, differences between altimetry sea level variations and those seen by tide gauge (see Eq.
4) can be related to Vertical Land Motion (VLM) at the tide gauge site (Wöppelmann and Marcos, 2016). We therefore
400 analysed the linear trend estimated on our altimeter bias time series to compare with the vertical motions of nearby GNSS
stations. A review of the GNSS stations in New Caledonia and the associated trend estimates is available in Appendix A. While
we do not obtain significant trends over Jason 2 and Jason 3 periods, our results show a subsidence of – 4 ± 1 mm/y for the
Jason 1 period [2002-2008]. At this time, the VLM estimates at NOUM permanent GNSS station also show a subsidence (e.g.
a trend estimates of -2.5 ± 0.5 mm/y over [2000-2007] with the SONEL-ULR7 solution). However, this value varies greatly
405 depending on the time-span and the solutions considered (see Table A2 and Fig. A3), and further investigations are needed to
explain this subsidence (remaining errors in the altimetry process, more robust trend estimates over this period, etc.).

As detailed in Section 2.2 and Appendix A, the question of long-term sea level evolution in the Lagoon is not fully resolved.
With the 20 years of altimeter and tide gauge differences, we are able to estimate our own trend. First, we realign the 3 bias
410 time series by applying the mean biases computed in this paper (i.e. -66mm for J1, -39mm for J2, -12mm for J3) (Fig. 9b). To
have a more robust estimate of the trend, we then used a bootstrapping method, which consists in estimating the trend 200
times on a random sample of 85% of the original series. Over the whole Jason period [2002-2022], we obtain a linear trend of
-0.2 ± 0.1 mm/year. It is important to note that this trend is sensitive to the biases applied: for example, using Bass Strait mean
biases (i.e. -41/-15/+4 mm instead of -66/-39/-12 mm), we find a trend of -0.7 ± 0.1mm/y.

415

This being said, our results do not show any significant uplift in Noumea. This differs from the conclusions of Aucan et al.
(2017), that find an uplift of +1.41 ±0.67 mm/y over the altimetric period [1993-2013] inferred from the difference between
satellite altimetry and tide gauge. The difference likely originates in the method used by Aucan et al. (2017), where the satellite
altimetry time series was extracted from a multi-mission gridded dataset at a point far outside the lagoon, before being
420 compared to the tide gauge (see Figure A4 in Appendix A). Section 4.2.2 showed that, even being only a few km apart, there

is SSH differences between the tide gauge and the pressure sensor: the difference with a point outside the lagoon can therefore be even greater. Other studies that compare altimetry and tide gauges also find a significant uplift in the area (resp. 1.7 ± 0.2 and 2.5 ± 1.5 mm/y for Nerem and Mitchum, 2002 and Martínez-Asensio et al., 2019). By using along track altimetry products and a closer comparison point, our approach led to a slightly different conclusion.

425

Regarding VLM estimates from GNSS permanent stations, one thing to note is that most of them highlight a small subsidence in New-Caledonia (see Appendix A). For example, thanks to the combined results of multiple computing centres, Ballu et al. (2019) found an average subsidence of -1.3 ±0.3 mm/y in Noumea . However, authors also show that this VLM estimation can be very sensitive to the integration (or not) of a discontinuity in the time series. To solve the question of long-term sea level
430   change in the lagoon, further studies are thus needed on GNSS data analysis as well as on altimetry and tide gauges. For

Figure 9. (a) Altimeter bias time series at the comparison point for Jason 1 (red), Jason 2 (green) and Jason 3 (orange) track #162. / (b) Altimeter bias time series after applying mean biases found in this study (i.e. -66mm for J1, -39mm for J2 and -12mm for J3). The black line represents the resulting trend compute over the whole Jason period [2002-2022].

example, extending our time series with TOPEX/Poseidon or Sentinel-6 observations would give us a longer and more robust trend estimate. Having longer observations from the GNSS permanent station collocated with Numbo tide gauge could also help to constrained vertical land movements at tide gauge.

5. Conclusion

435 In this paper, we demonstrate the potential of the New Caledonia lagoon near Noumea to host Cal/Val activities. Using *in situ* data acquired as part of the GEOCEAN-NC campaign, this study proposes a method to link and compare observations from the Noumea long-term tide gauge site and an offshore altimetry crossover point from Jason and Sentinel-3a missions. Thanks to the measurements of a GNSS buoy and a bottom pressure sensor, we are able to virtually transfer long-term Noumea tide gauge data at this altimeter crossover. A comparison over the common year of measurement of the tide gauge and the pressure

440 sensor show that this method is relevant for estimating altimeter bias at the cm-level. The use of along-track altimetry product allows us to test and adapt altimeter correction parameters, especially for the wet tropospheric delay. We consider the up-to-date GDR parameters and thanks to a CalNaGeo survey, we validated the use of the XGM2019 gravity field model to account for geoid gradients.

445 Following the philosophy of Cal/Val studies, we are thus able to compute a precise absolute altimeter bias time series. For the 3 Jason missions and Sentinel-3a, we find mean altimeter biases slightly higher than other historical Cal/Val sites estimates, except for Jason 3 mean bias which is close to the Harvest one. Our estimates of the inter-mission biases are also consistent, especially with the results of the Bass Strait site (see Table 3). These results are very encouraging, despite the uncertainties about the vertical referencing of our *in situ* observations (see Section 4.2.3). Additional geodetic measurements with buoys

450 and pressure sensors at the crossover location could help to control and consolidate this vertical datum. In the future, this site also gives the opportunity to reanalyse data from the TOPEX/Poseidon to the recent Sentinel-6 missions. Extending the comparison will allow to answer new questions, and particularly try to reconcile the sea level trends seen by altimetry, tide gauges and terrestrial permanent GNSS stations. One could also consider transposing this method to other study areas, thus increasing the potential number of Cal/Val studies around the world. However, in addition to enabling the deployment of

455 offshore geodetic campaigns, these potential sites require having suitable altimetry measurement in the vicinity of a reliable sea level observatory (e.g. a long-term tide gauge site), and a good knowledge of the local geophysical and hydrodynamic context to account for the difference in oceanographic signals.

Finally, although the GEOCEAN-NC campaign is not directly related to the preparation of the future SWOT mission, a better

460 knowledge of the lagoon dynamics and the mapping of the fine-scale geoid will be useful for the exploitation of its future large-swath measurements. Thus, the Noumea lagoon represents a real opportunity to establish an absolute and relatively low-cost Cal/Val site, to better understand current and future altimetry data.

Table 3. Altimetric mean biases and inter-mission biases for Jason 1-2-6 and Sentinel-3a missions for three historical Cal/Val sites and the Noumea lagoon (Harvest, Corsica and Bass Strait results are extract from the last OSTST sessions - Bonnefond et al., 2022a)

		Jason 1	Jason 2	Jason 3	Sentinel-3a
Harvest	*Products*	GDR-E	GDR-D	GDR-F	-
	Bias	+12 ± 2 mm	+8 ± 2 mm	+14 ± 2 mm	-
	Inter-mission	-	-1 mm	+6 mm	-	-

		Jason 1	Jason 2	Jason 3	Sentinel-3a
Corsica	*Products*	GDR-E	GDR-D	GDR-F	PDGS
	Bias	+43 ± 3 mm	+16 ± 2 mm	+4 ± 2 mm	+22 ± 4 mm
	Inter-mission	-	-27 mm	-12 mm	+18 mm	-

		Jason 1	Jason 2	Jason 3	Sentinel-3a
Bass Strait	*Products*	GDR-E	GDR-D	GDR-F	NTC, BC4/BC5
	Bias	+41 ± 2 mm	+15 ± 2 mm	-4 ± 2 mm	+25 ± 2 mm
	Inter-mission	-	-26 mm	-19 mm	+29 mm	-

		Jason 1	Jason 2	Jason 3	Sentinel-3a
Noumea	*Products*	GDR-E	GDR-D	GDR-F	NTC, BC4
	Cycles	1-259	1-303	1-219	3-81
	Bias	+66 ± 2 mm	+39 ± 3 mm	+12 ± 3 mm	+40 ± 4 mm (#359) +39 ± 3 mm (#458)
	Inter-mission	-	-27 mm	-27 mm	+28 mm	-

Author contribution

C.C., V.B., L.T. and Y.-T.T. designed the study, V.B, C.C. and J.A. designed and conducted the field campaign, C.C. processed the data and wrote the original draft of the paper. Writing—review & editing, C.C., V.B., L.T., Y.-T.T. and J.A. All authors have read and agreed to the published version of the manuscript.

Data availability

Navigation data for the 2019 GEOCEAN-NC campaign are available online (https://doi.org/10.17600/18000899). Altimetry products are available for download online (see Section 4.1.1) and sensor data used in this paper are available from the authors upon request.

Competing interests

The authors declare no conflict of interest. The funders had no role in the design of the study; in the collection, analyses, or interpretation of data; in the writing of the manuscript, or in the decision to publish the results.

Funding

This study has been conducted and funded thanks to Centre National d'Etudes Spatiales (CNES) through the FOAM project of the TOSCA program, Centre National de la Recherche Scientifique (CNRS), and French Ministry of Research. Funding for C.Chupin PhD is provided by the Direction Générale de l'Armement (DGA) and the Nouvelle Aquitaine region.

Acknowledgements

485   For the GEOCEAN-NC mission in Noumea lagoon in October 2019 (DOI : https://doi.org/10.17600/18000899), the authors want to thank Etienne Poirier for the instrument management during the campaign, and the commandant and crew of the R/V Alis. We acknowledge the help of IRD, Shom and DITTT for logistics and on-land tide and GNSS data collection. We also thank the US IMAGO Noumea teams for their logistic support during the campaign, and more particularly Bertrand Bourgeois and Mahé Dumas for the deployment and recovery of the pressure sensors. We acknowledge the CNFC (Comission Nationale

490   de la Flotte Côtière), Ifremer, IRD and the Government of New Caledonia for rapidly adjusting and obtaining permissions for the new cruise plan. We also want to thanks the GINS community and especially the GET laboratory for helping with GNSS computation, and the LEGOS altimetry experts (especially Florence Birol and Fabien Léger) for their help and advices analysing altimetry dataset in the lagoon. The pressure sensor data were analysed using code kindly provided by Marc Pezerat from LIENSs. We would like to thank the anonymous reviewer for his pertinent comments, as well as Christopher Watson for

495   his detailed proofreading which allowed us to point out inconsistencies and omissions in the original paper, and certainly improve the quality of our study.

References

Ablain, M., Cazenave, A., Valladeau, G., and Guinehut, S.: A new assessment of the error budget of global mean sea level rate estimated by satellite altimetry over 1993–2008, Ocean Sci., 5, 193–201, https://doi.org/10.5194/os-5-193-2009, 2009.

500 Ablain, M., Meyssignac, B., Zawadzki, L., Jugier, R., Ribes, A., Spada, G., Benveniste, J., Cazenave, A., and Picot, N.: Uncertainty in satellite estimates of global mean sea-level changes, trend and acceleration, Earth Syst. Sci. Data, 11, 1189–1202, https://doi.org/10.5194/essd-11-1189-2019, 2019.

Andersen, O. B. and Scharroo, R.: Range and Geophysical Corrections in Coastal Regions: And Implications for Mean Sea Surface Determination, in: Coastal Altimetry, edited by: Vignudelli, S., Kostianoy, A. G., Cipollini, P., and Benveniste, J., 505 Springer Berlin Heidelberg, Berlin, Heidelberg, 103–145, https://doi.org/10.1007/978-3-642-12796-0_5, 2011.

André, G., Miguez, B. M., Ballu, V., Testut, L., and Wöppelmann, G.: Measuring sea level with GPS-equipped buoys: a multi-instruments experiment at Aix Island, Int. Hydrogr. Rev., 26–38, https://journals.lib.unb.ca/index.php/ihr/article/view/22826, 2013.

Aucan, J., Merrifield, M. A., and Pouvreau, N.: Historical Sea Level in the South Pacific from Rescued Archives, Geodetic 510 Measurements, and Satellite Altimetry, Pure Appl. Geophys., 174, 3813–3823, https://doi.org/10.1007/s00024-017-1648-1, 2017.

Ballu, V.: GEOCEAN-NC cruise - RV Alis, https://doi.org/10.17600/18000899, 2019.

Ballu, V., Gravelle, M., Woppelmann, G., de Viron, O., Rebischung, P., Becker, M., and Sakic, P.: Vertical land motion in the Southwest and Central Pacific from available GNSS solutions and implications for relative sea levels, Geophys. J. Int., 218, 515 1537–1551, https://doi.org/10.1093/gji/ggz247, 2019.

Bonnefond, P., Haines, B. J., and Watson, C.: In situ Absolute Calibration and Validation: A Link from Coastal to Open-Ocean Altimetry, in: Coastal Altimetry, edited by: Vignudelli, S., Kostianoy, A. G., Cipollini, P., and Benveniste, J., Springer Berlin Heidelberg, Berlin, Heidelberg, 259–296, https://doi.org/10.1007/978-3-642-12796-0_11, 2011.

Bonnefond, P., Exertier, P., Laurain, O., Thibaut, P., and Mercier, F.: GPS-based sea level measurements to help the 520 characterization of land contamination in coastal areas, Adv. Space Res., 51, 1383–1399, https://doi.org/10.1016/j.asr.2012.07.007, 2013.

Bonnefond, P., Exertier, P., Laurain, O., Guinle, T., and Féménias, P.: Corsica: A 20-Yr multi-mission absolute altimeter calibration site, Adv. Space Res., S0273117719307276, https://doi.org/10.1016/j.asr.2019.09.049, 2019.

Bonnefond, P., Haines, B., Legresy, B., and Watson, C.: Absolute calibration results from Bass Strait, Corsica, and Harvest 525 facilities, OSTST Meeting Venice, 2022a.

Bonnefond, P., Laurain, Olivier., Exertier, P., Calzas, M., Guinle, T., Picot, N., and the FOAM Project Team: Validating a New GNSS-Based Sea Level Instrument (CalNaGeo) at Senetosa Cape, Mar. Geod., 45, 121–150, https://doi.org/10.1080/01490419.2021.2013355, 2022b.

Born, G. H., Parke, M. E., Axelrad, P., Gold, K. L., Johnson, J., Key, K. W., Kubitschek, D. G., and Christensen, E. J.: 530 Calibration of the TOPEX altimeter using a GPS buoy, J. Geophys. Res., 99, 24517, https://doi.org/10.1029/94JC00920, 1994.

Cazenave, A., Palanisamy, H., and Ablain, M.: Contemporary sea level changes from satellite altimetry: What have we learned? What are the new challenges?, Adv. Space Res., 62, 1639–1653, https://doi.org/10.1016/j.asr.2018.07.017, 2018.

Chelton, D. B., Ries, J. C., Haines, B. J., Fu, L.-L., and Callahan, P. S.: Satellite altimetry, Satell. Altimetry Earth Sci., 69, 1–131, 2001.

535 Chupin, C., Ballu, V., Testut, L., Tranchant, Y.-T., Calzas, M., Poirier, E., Coulombier, T., Laurain, O., Bonnefond, P., and Team FOAM Project: Mapping Sea Surface Height Using New Concepts of Kinematic GNSS Instruments, Remote Sens., 12, 2656, https://doi.org/10.3390/rs12162656, 2020.

Douillet, P.: Tidal dynamics of the south-west lagoon of New Caledonia: observations and 2D numerical modelling, Oceanol. Acta, 21, 69–79, https://doi.org/10.1016/S0399-1784(98)80050-9, 1998.

540 Escudier, P., Couhert, A., Mercier, F., Mallet, A., Thibaut, P., Tran, N., Amarouche, L., Picard, B., Carrere, L., Dibarboure, G., Ablain, M., Richard, J., Steunou, N., Dubois, P., Rio, M.-H., and Dorandeu, J.: Satellite Radar Altimetry: Principle, Accuracy, and Precision, in: Satellite Altimetry Over Oceans and Land Surfaces, CRC Press, 2017.

Fu, L.-L. and Haines, B. J.: The challenges in long-term altimetry calibration for addressing the problem of global sea level change, Adv. Space Res., 51, 1284–1300, https://doi.org/10.1016/j.asr.2012.06.005, 2013.

545 Fund, F., Perosanz, F., Testut, L., and Loyer, S.: An Integer Precise Point Positioning technique for sea surface observations using a GPS buoy, Adv. Space Res., 51, 1311–1322, https://doi.org/10.1016/j.asr.2012.09.028, 2013.

GCOS: GCOS Essential Climate Variables Requirements, World Meteorological Organization (WMO), 2022.

Gobron, K., de Viron, O., Wöppelmann, G., Poirier, É., Ballu, V., and Van Camp, M.: Assessment of Tide Gauge Biases and Precision by the Combination of Multiple Collocated Time Series, J. Atmospheric Ocean. Technol., 36, 1983–1996, 550 https://doi.org/10.1175/JTECH-D-18-0235.1, 2019.

Gommenginger, C., Thibaut, P., Fenoglio-Marc, L., Quartly, G., Deng, X., Gómez-Enri, J., Challenor, P., and Gao, Y.: Retracking Altimeter Waveforms Near the Coasts, in: Coastal Altimetry, edited by: Vignudelli, S., Kostianoy, A. G., Cipollini, P., and Benveniste, J., Springer Berlin Heidelberg, Berlin, Heidelberg, 61–101, https://doi.org/10.1007/978-3-642-12796-0_4, 2011.

555 Gourdeau, L., Cravatte, S., and Marin, F.: SWOT in the Tropics - Internal tides and mesoscale interactions in a tropical area: insights from model, in situ data and SWOT, 2020.

Haasnoot, M., Winter, G., Brown, S., Dawson, R. J., Ward, P. J., and Eilander, D.: Long-term sea-level rise necessitates a commitment to adaptation: A first order assessment, Clim. Risk Manag., 34, 100355, https://doi.org/10.1016/j.crm.2021.100355, 2021.

560 Haines, B., Desai, S. D., Kubitschek, D., and Leben, R. R.: A brief history of the Harvest experiment: 1989–2019, Adv. Space Res., S0273117720305718, https://doi.org/10.1016/j.asr.2020.08.013, 2020.

Hersbach, H., Bell, B., Berrisford, P., Biavati, G., Horányi, A., Muñoz Sabater, J., Nicolas, J., Peubey, C., Radu, R., Rozum, I., Schepers, D., Simmons, A., Soci, C., Dee, D., and Thépaut, J.-N.: ERA5 hourly data on pressure levels from 1979 to present, Copernicus Climate Change Service (C3S) Climate Data Store (CDS), 2018.

565 Imel, D. A.: Evaluation of the TOPEX/POSEIDON dual-frequency ionosphere correction, J. Geophys. Res., 99, 24895, https://doi.org/10.1029/94JC01869, 1994.

Jason-3 Products Handbook, CNES, EUMETSAT, JPL, NOAA, 2020.

Legeais, J.-F., Ablain, M., Zawadzki, L., Zuo, H., Johannessen, J. A., Scharffenberg, M. G., Fenoglio-Marc, L., Fernandes, M. J., Andersen, O. B., Rudenko, S., Cipollini, P., Quartly, G. D., Passaro, M., Cazenave, A., and Benveniste, J.: An improved and homogeneous altimeter sea level record from the ESA Climate Change Initiative, Earth Syst. Sci. Data, 10, 281–301, https://doi.org/10.5194/essd-10-281-2018, 2018.

Martínez-Asensio, A., Wöppelmann, G., Ballu, V., Becker, M., Testut, L., Magnan, A. K., and Duvat, V. K. E.: Relative sea-level rise and the influence of vertical land motion at Tropical Pacific Islands, Glob. Planet. Change, 176, 132–143, https://doi.org/10.1016/j.gloplacha.2019.03.008, 2019.

Marty, J. C., Loyer, S., Perosanz, F., Mercier, F., Bracher, G., Legresy, B., Portier, L., Capdeville, H., Fund, F., Lemoine, J. M., and Biancale, R.: GINS: The CNES/GRGS GNSS scientific software, in: ESA Proceedings WPP326, 3 rd International Colloquium Scientific and Fundamental Aspects of the Galileo Programme, Copenhagen, Denmark, 2011.

Mertikas, S., Donlon, C., Féménias, P., Mavrocordatos, C., Galanakis, D., Tripolitsiotis, A., Frantzis, X., Tziavos, I., Vergos, G., and Guinle, T.: Fifteen Years of Cal/Val Service to Reference Altimetry Missions: Calibration of Satellite Altimetry at the Permanent Facilities in Gavdos and Crete, Greece, Remote Sens., 10, 1557, https://doi.org/10.3390/rs10101557, 2018.

Mitchum, G. T.: An Improved Calibration of Satellite Altimetric Heights Using Tide Gauge Sea Levels with Adjustment for Land Motion, Mar. Geod., 23, 145–166, https://doi.org/10.1080/01490410050128591, 2000.

Nerem, R. S. and Mitchum, G. T.: Estimates of vertical crustal motion derived from differences of TOPEX/POSEIDON and tide gauge sea level measurements, Geophys. Res. Lett., 29, 40-1-40–4, https://doi.org/10.1029/2002GL015037, 2002.

Nerem, R. S., Haines, B. J., Hendricks, J., Minster, J. F., Mitchum, G. T., and White, W. B.: Improved determination of global mean sea level variations using TOPEX/POSEIDON altimeter data, Geophys. Res. Lett., 24, 1331–1334, https://doi.org/10.1029/97GL01288, 1997.

Oppenheimer, M., Glavovic, B. C., Hinkel, J., van de Wal, R., Magnan, A. K., Abd-Elgawad, A., Cai, R., Cifuentes-Jara, M., Rica, C., DeConto, R. M., Ghosh, T., Hay, J., Islands, C., Isla, F., Marzeion, B., Meyssignac, B., Sebesvari, Z., Biesbroek, R., Buchanan, M. K., de Campos, R. S., Cozannet, G. L., Domingues, C., Dangendorf, S., Döll, P., Duvat, V. K. E., Edwards, T., Ekaykin, A., Frederikse, T., Gattuso, J.-P., Kopp, R., Lambert, E., Lawrence, J., Narayan, S., Nicholls, R. J., Renaud, F., Simm, J., Smit, A., Woodruff, J., Wong, P. P., Xian, S., Abe-Ouchi, A., Gupta, K., and Pereira, J.: Sea Level Rise and Implications for Low-Lying Islands, Coasts and Communities, IPCC Spec. Rep. Ocean Cryosphere Chang. Clim., 126, 2019.

Petit, G. and Luzum, B.: IERS Conventions, International Earth Rotation and Reference Systems Service (IERS), 2010.

Prandi, P., Meyssignac, B., Ablain, M., Spada, G., Ribes, A., and Benveniste, J.: Local sea level trends, accelerations and uncertainties over 1993–2019, Sci. Data, 8, 1, https://doi.org/10.1038/s41597-020-00786-7, 2021.

Vondrak, J.: Problem of Smoothing Observational Data II, Astron. Institue Czechoslov. Acad. Sci. Praha, 28, 84–89, 1977.

Watson, C., White, N., Church, J., Burgette, R., Tregoning, P., and Coleman, R.: Absolute Calibration in Bass Strait, Australia: TOPEX, Jason-1 and OSTM/Jason-2, Mar. Geod., 34, 242–260, https://doi.org/10.1080/01490419.2011.584834, 2011.

Willis, J.: Report of the 2011 Ocean Surface Topography Science Team Meeting., 2011.

Wöppelmann, G. and Marcos, M.: Vertical land motion as a key to understanding sea level change and variability: Vertical Land Motion and Sea Level Change, Rev. Geophys., 54, 64–92, https://doi.org/10.1002/2015RG000502, 2016.

Zhang, Y. J., Ye, F., Stanev, E. V., and Grashorn, S.: Seamless cross-scale modeling with SCHISM, Ocean Model., 102, 64–81, https://doi.org/10.1016/j.ocemod.2016.05.002, 2016.

605 Zhou, B., Watson, C., Legresy, B., King, M. A., Beardsley, J., and Deane, A.: GNSS/INS-Equipped Buoys for Altimetry Validation: Lessons Learnt and New Directions from the Bass Strait Validation Facility, Remote Sens., 12, 3001, https://doi.org/10.3390/rs12183001, 2020.

Zhou, B., Watson, C., Legresy, B., King, M. A., and Beardsley, J.: Ongoing Development of the Bass Strait GNSS/INS Buoy System for Altimetry Validation in Preparation for SWOT, Remote Sens., 15, 287, https://doi.org/10.3390/rs15010287, 2023.

610 Zingerle, P., Pail, R., Gruber, T., and Oikonomidou, X.: The combined global gravity field model XGM2019e, J. Geod., 94, 66, https://doi.org/10.1007/s00190-020-01398-0, 2020.

Zumberge, J. F., Heflin, M. B., Jefferson, D. C., Watkins, M. M., and Webb, F. H.: Precise point positioning for the efficient and robust analysis of GPS data from large networks, J. Geophys. Res. Solid Earth, 102, 5005–5017, https://doi.org/10.1029/96JB03860, 1997.

615

Appendices

20   Appendix A - Geophysical situation of the Noumea Lagoon

This appendix gives the geophysical context of our study based on the scientific litterature.

Global geophysical context (from Ballu et al., 2019)

Ballu et al. (2019) details the geophysical context of the South West Pacific zone (see Figure A1 for an overview). Focusing on our study area, the Noumea Lagoon is on an active tectonic zone on the Indo-Australian plate, that converge to the Pacific one at a mean rate of about 10 cm/y. There are two major subduction zones, and Noumea is near the New Hebrides and Papoua-New Guinea—Salomon one, where the Australian plate is subducting. The contribution of non-tectonic processes to vertical displacement (i.e. subsidence of Pacific volcanoes and post-glacial isostatic adjustment) is estimated to be less than 1mm/y. It also appears that Noumea could be affected by earthquake, although neither strongly nor frequently.
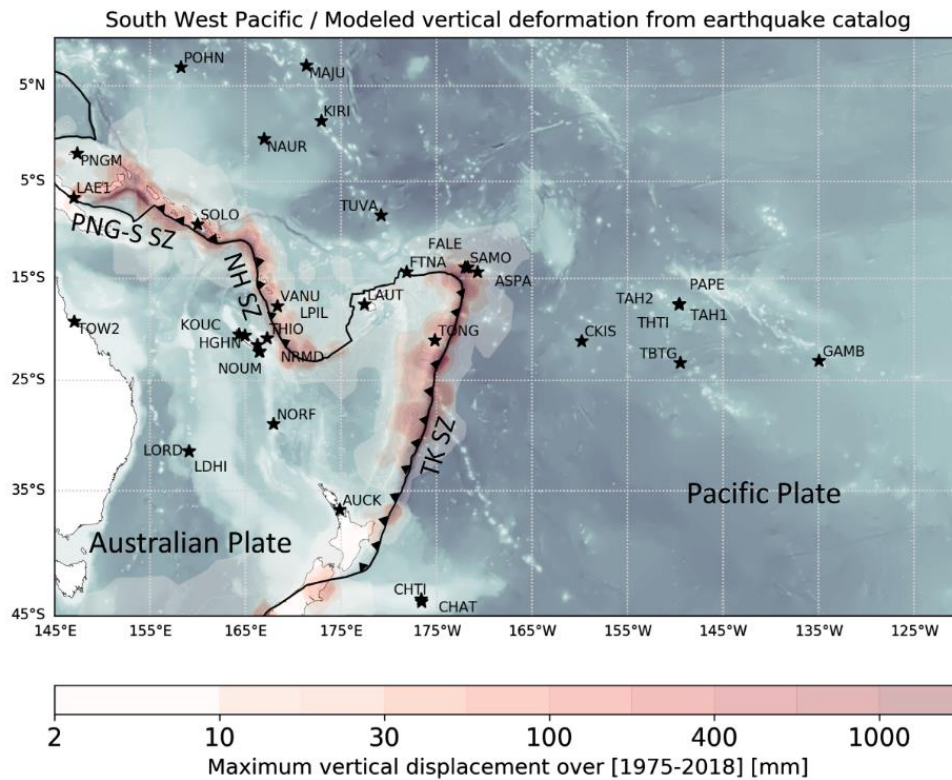
Figure A1. Extracted from Ballu et al. (2019) – *Stars represent stations with a long enough GPS record available (~7 yr). The background grey/blue shading highlights the bathymetric features in the oceanic domain, based on GEBCO 2014 (Weatherall et al., 2015) bathymetric data. The red shading indicates maximum absolute values of vertical displacement modelled using Okada (1985) dislocation model and the USGS earthquakes catalog for the period 1975–2018. The black line corresponds to the tectonic plate limit between the Australian Plate and the Pacific Plate, as proposed in the Morvel-25 plate boundary model (DeMets et al., 2010). The subduction zones are indicated by triangles on the over-riding plate, and labelled TK SZ, NH SZ and PNG-S SZ, respectively for the Tonga-Kermadec, New Hebrides and Papoua-New Guinea—Salomon subduction zones.*

Global and local hydrodynamic context

40   There is a strong sea level regional variability in the western tropical Pacific area, mainly linked to the ENSO (El Niño-Southern Oscillation) with lower (resp. higher) sea level during El Niño (resp. La Nina) events, with differences in sea level around ± 20-30 cm (Becker et al., 2012). From the study of Garcin et al. (2016), it appears that periods that combine La Nina events and a negative Interdecadal Pacific Oscillation (IPO) lead to stronger trade winds and higher sea levels in the Lagoon. The climate component of sea level rise in Noumea is estimated to be around +0.5 ± 0.5 mm/y (Becker et al., 2012).

The lagoon surrounding New Caledonia is the world's largest lagoon, covering about 20,000 km². A barrier reef separates the lagoon from the Pacific Ocean, at a distance from the coast ranging from 5 km in its northern part to 40 km in its southern part. Deep passes intersect the coral reef and let the ocean flow in and out. During low tides, the crest of the reef can emerge.

50   The southern part of the lagoon, near Noumea city has an average depth of 15-20 m. Its dynamics is dominated by semi-diurnal tides, with a tidal range varying from about 1.4 m at spring tides to 0.6 m at neap tides (Douillet, 1998). Part of the offshore oceanic signal enters the lagoon through deep passes, but it is then strongly attenuated inside the Lagoon by wave breaking and friction on the reef flat (Bonneton et al., 2007).

55   To a first approximation, the sea state in the lagoon is mainly dominated by the wind sea (Jouon et al., 2009). Aucan et al. (2017b) identify three types of waves in the lagoon: (1) low-frequency swell waves (8-25 s) generated offshore (SSW) and then impacting the barrier reef, (2) high-frequency waves (3-8 s), generated inside the lagoon by the prevailing trade winds (SE), and (3) infragravity waves (20-500 s) that can be similarly energetic on the islet reef flat. The wave impact on the islands depend on their location and distance to the coral reef and the main passes, and is modulated by tidal level and the surrounding
60   reef plate (Aucan et al., 2017b; Garcin et al., 2016).

Finally, it is possible that wave breaking on the barrier reef could induce a localized elevation of the water body behind the reef (i.e. setup), which would be evacuated through the passes and would not necessarily reach the coast and thus the tide gauge. This phenomenon was observed during the passage of tropical cyclone COOK in 2017 (Jullien et al., 2020). However,
65   in previous publication based on in-situ data in the lagoon (Aucan et al., 2017b), no significant setup was observed (Aucan pers. communication).

Sea level trends and vertical land movements in New Caledonia

In New-Caledonia, the sea level evolution is still an issue as altimetry, tide gauge and land-based GNSS station do not provide consistent information (Aucan et al., 2017a, Martínez-Asensio et al., 2019 and tables A1 and A2 for an overview of the values).
70   Over the altimetry period (1993-2013), Aucan et al. (2017a) find a sea level trend difference between tide gauge and altimetry

of +1.4 ± 0.7 mm/y. Ideally, these residuals movements could be explained by Vertical Land Movements (VLM). However, nor VLM estimated by GIA models (i.e. ~ −0.1 to −0.3 mm/y in the area from the ICE6G-VM5a model - Peltier et al., 2015), nor VLM estimation from permanent GNSS stations (Table A2), could explain the uplift inferred by altimetry minus tide gauge measurements.

75

Several hypotheses could be considered to explain this:

1. A water level elevation between the altimeter sampling point and the tide gauge position (i.e. setup), which does not appear to be significant in the lagoon (see previous section for more details).

2. Mis-modeled discontinuities in the GNSS time series can result in an incorrect estimate of VLM. In their comparative study of different GNSS solutions, Ballu et al. (2019) find that the estimation of VLM trend for the NRMD station is very sensitive to the integration (or not) of a discontinuity during a material change in the middle of the time series. The methodology used to compute the trend and the period considered also impact the final result (see Table A2 and figure A2 for the different estimates of VLM at GNSS stations, and Figure A3 for time series comparison at NOUM station).

3. We can also consider the processing of altimetry data. For now, the data used in the tide gauge comparison are derived from gridded products integrating standard corrections that may not be appropriate for coastal locations. Aucan et al. (2017) altimeter point selected for comparison is located 95 km from the tide gauge. When considering the variability of sea level trends seen by altimetry in this area (Figure A4), one wonders if the selection of a point so far from the tide gauge is appropriate.

90
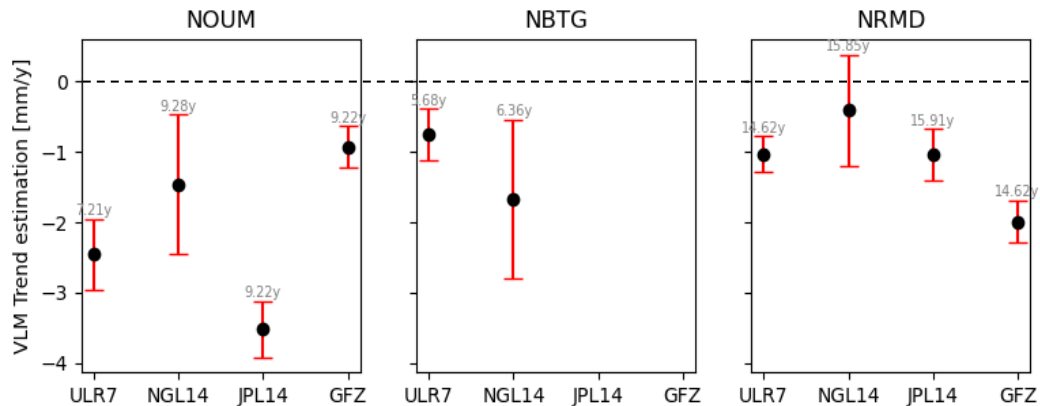
Figure A2. VLM trend estimation at three GNSS station in Noumea from 4 different solutions : SONEL-ULR7 solution from Gravelle et al. (2022) / NGL - NGL14 solution from Blewitt et al. (2016) / JPL - JPL14 solution from Heflin et al. (2020) / GFZ – GT3 solution from Männel et al. (2022). The red bar represents the uncertainty associated with each estimate, and the number shows the length of the observation years used to estimate the trend.

Table A1. Tide gauges Relative Sea Level trends estimates in New Caledonia from different studies

		Station name	Period	Trend [mm/y]	Source
Relative Sea Level	TG	Noumea	1957-2015	0.8 ± 0.4	Aucan et al., 2017a
			1993-2015	2.2 ± 1.6	
		Noumea A	1967-2015	0.9 ± 0.4	Martínez-Asensio et al., 2019
			1993-2015	2.4 ± 1.0	
		Ouinne	1981-2015	1.7 ± 0.3	
		Lifou	2011-2015	-5.0 ± 9.7	
	RESL[1] - GNSS	Noumea	1967-2003	2.6 ± 0.6	Becker et al., 2012

100

Table A2. Vertical Land Movements trends estimates in New Caledonia from different studies.

		Station name	Period	Trend [mm/y]	Source
Vertical Land Movements	GNSS	NOUM	1997-2007	-1.4 ± 0.3	Martínez-Asensio et al., 2019
			-	-2.1 ± 0.2	Becker et al., 2012
			-	-1.3 ± 0.7	Ballu et al., 2019
			2000-2007	-2.5 ± 0.5	SONEL – ULR7 [2]
			1998-2007	-1.5 ± 1.0	NGL - NGL14 [2]
			1998-2007	-3.5 ± 0.4	JPL - JPL14 [2]
			1998-2007	-0.9 ± 0.3	GFZ – GT3 [2]
			1998-2007	-1.5 ± 1.0	Hammond et al., 2021
		NRMD	-	-1.3 ± 0.6	Ballu et al., 2019
			2006-2020	-1.0 ± 0.3	SONEL – ULR7 [2]
			2006-2021	-0.4 ± 0.8	NGL - NGL14 [2]
			2006-2021	-1.0 ± 0.4	JPL - JPL14 [2]
			2006-2020	-2.0 ± 0.3	GFZ – GT3 [2]
			2006-2023	-0.5 ± 0.6	Hammond et al., 2021
		NBTG	2015-2020	-0.7 ± 0.4	SONEL – ULR7 [2]
			2015-2021	-1.7 ± 1.1	NGL - NGL14 [2]
			2015-2022	-1.7 ± 1.2	Hammond et al., 2021
		YATE	2008-2016	1.7 ± 1.7	Martínez-Asensio et al., 2019
		LPIL	1996-2016	-0.2 ± 0.4	
			-	-0.7 ± 0.7	Ballu et al., 2019
		THIO	-	-2.0 ± 0.7	
			2008-2023	-1.8 ± 1.2	Hammond et al., 2021
		KOUC	-	-0.9 ± 0.6	Ballu et al., 2019

---

[1] RESL = Reconstructed Sea Level (see Becker et al., 2012 for more details)
[2] GNSS VLM sources : SONEL-ULR7 solution from Gravelle et al. (2022) / NGL - NGL14 solution from Blewitt et al. (2016) / JPL - JPL14 solution from Heflin et al. (2020) / GFZ – GT3 solution from Männel et al. (2022)

		HGHN	-	-1.3 ± 0.6	
			2010-2023	-1.7 ± 1.2	Hammond et al., 2021
Altimetry-TG	Noumea		1993-2013	1.4 ± 0.7	Aucan et al., 2017a
			1957-2010	1.4 ± 0.4	
			1993-2001	2.5 ± 1.5	Nerem and Mitchum, 2002
			1967-2015	1.7 ± 0.2	Martínez-Asensio et al., 2019
VLM@TG *(from GNSS station interpolation)*	Chaleix		-	-1.7 ± 0.3	Hammond et al., 2021
	Numbo		-	-1.7 ± 0.4	
	Ouinne		-	-1.8 ± 0.4	
	Lifou		-	-3.1 ± 1.1	
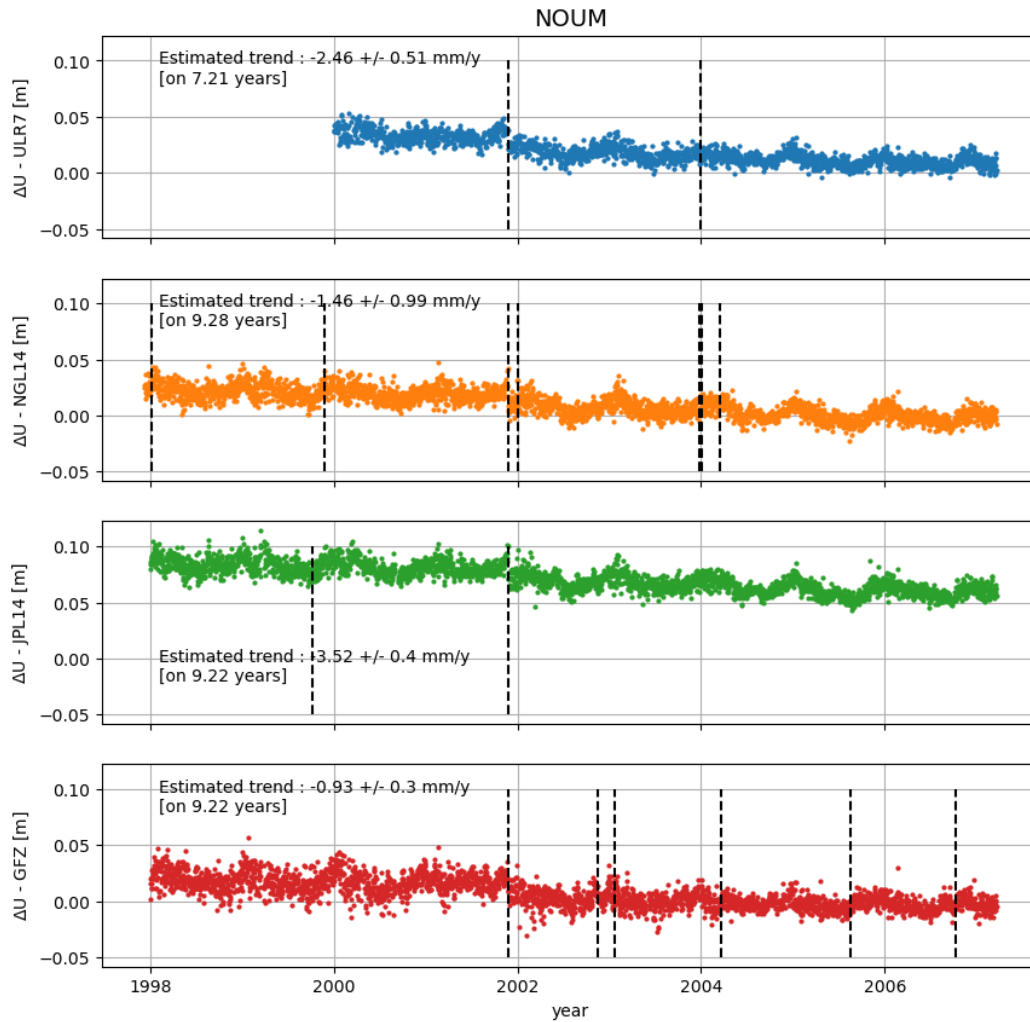
105

Figure A3. Time series used to estimate VLM trend at the NOUM station for the 4 solutions presented in Figure G2. The dashed vertical bar indicates the discontinuity considered by each solution to compute the final trend.
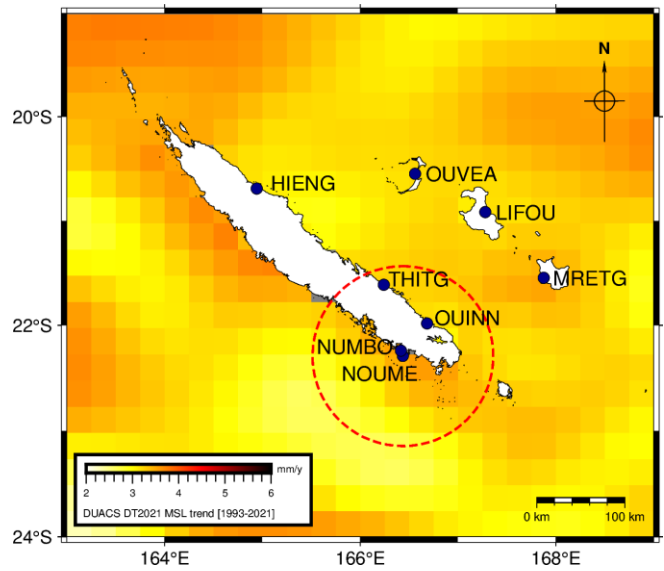
110

Figure A4. Location of the main TG sites in New-Caledonia. The background shows the merged gridded regional mean sea level trends from DUACS DT2021 over [1993-2021] (CLS/CMEMS). The red dotted circle with 95km radius represent the distance between Noumea tide gauge and altimetry grid node used in Aucan et al., 2017a study for comparison.
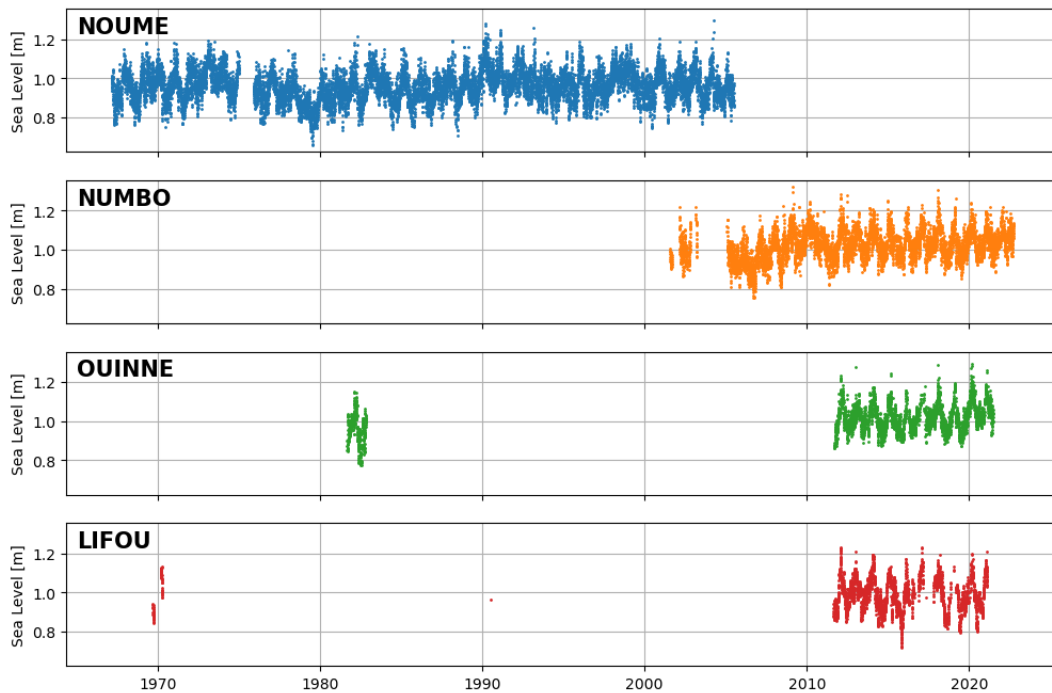
115

Figure A5. Overview NOUME/NUMBO/OUINNE/LIFOU tide gauges daily sea level means from SONEL portal.

Appendix B - Calibration of GEOCEAN-NC pressure gauges

Pressure sensors are known to drift over time. This drift is generally considered to be linear and variable from instrument to instrument, depending on the age and past history of the sensor. In our case, a calibration session in hyperbaric chamber before
120 and after their deployment do not show a clear instrumental drift of the different sensors (Figure B1c).

To verify the stability of the measurements during the 13 months of immersion, we compute relative differences with the 2019o sensor (Figure B1d). This sensor was chosen as a reference because of its installation on a stable support (coral reef), and we consider its instrumental drift negligible regarding the previous calibration session. Results show that, for sensors 2019i
125 and 2019j (Figure B1d, in green and yellow), differences do not show a significant trend: therefore, it is assumed that these two sensors remained stationary.

On the contrary, the 2019o/2019r difference (Figure B1d, in red) shows a negative trend for the first 7 months, before stabilizing in May 2020. This suggests a sinking of the sensor into the sand, which was confirmed by the divers during the
130 gauge's recovery. The nature of the bottom is therefore a parameter to consider when deploying the sensors. If the experimental conditions impose an installation on very soft grounds, other types of support can also be considered (suction anchors, etc.). Finally, the 2019o/2019x difference (Figure B1d, blue) shows a linear trend of about -70 mm/yr, which is not visible on the other sensors nor conceivable from the pre- and post-deployment drift checks. This could indicate continued sensor sinking, and in the absence of further information, we chose to correct for this trend in the following study.
135
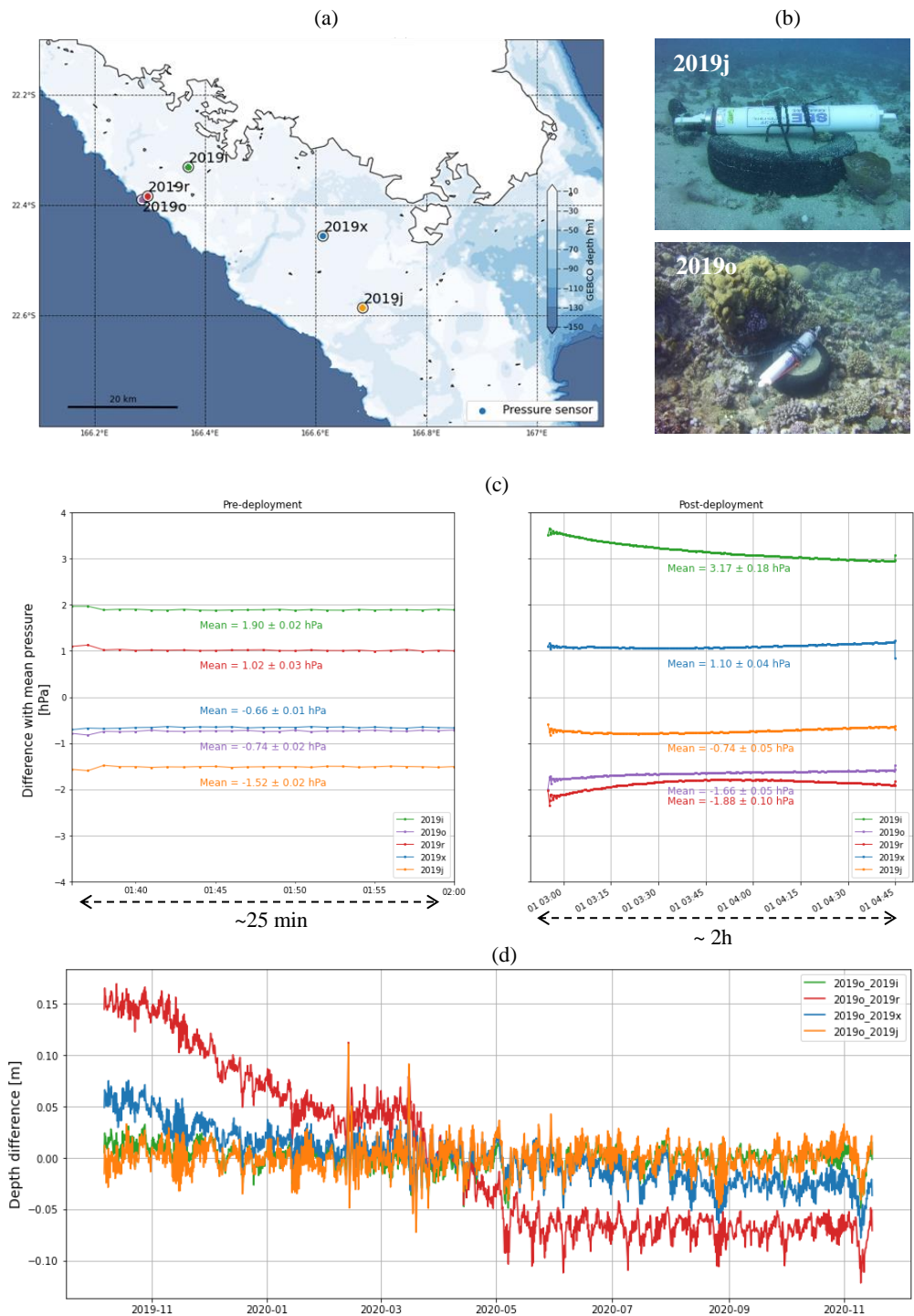
Figure B1. Installation and calibration phase of the pressure gauges / (a) – (b) Location and mooring of the 5 pressure gauges deployed during GEOCEAN-NC campaign. / (c) Hyperbaric chamber calibration results: difference between SBE observations and mean pressure at 10m before (left) and after (right) deployment. For conversion, 1 hPa ~ 1 cm of water. / (d) Difference between the 2019o sensor time series and the other 4 pressure sensors. The pressure time series were transformed into equivalent water depths and then corrected for tide using harmonic analysis. The final differences were filtered with a sliding average (6 h windows, 6 h steps).

Appendix C - GNSS processing parameters

Table C1. GINS parameters for GNSS computation[3]

	GNSS Buoy	CalNaGeo GNSS carpet
Antenna model	TRM115000.10 NONE	TRM125000.30 NONE
Receiver model	SEPT POLARX5	SEPT POLARX5
Constellation(s) used	GPS / GLONASS / GALILEO	GPS / GLONASS / GALILEO
Resolution mode	IPPP / PPP / IPPP	PPP
Observation sampling	10s (i.e. 1 obs./10s)	10s (i.e. 1 obs./10s)
Orbit/Clock products	MG3 *(30s products, linearly interpolated for higher frequencies data)*	MG3 *(30s products, linearly interpolated for higher frequencies data)*
Macromodel	Nominal MG3	Nominal MG3
ANTEX	igsR3_2077.atx	igsR3_2077.atx
Earth parameters	Nominal NRO	Nominal NRO
Ocean tide loading	FES2014	FES2014
Solid earth tide	IERS 2010 convention *(cyclic and permanent component)*	IERS 2010 convention *(cyclic and permanent component)*
Atmosphere loading	Uncorrected	Uncorrected
Ocean tide	Uncorrected	Uncorrected
Mean sea surface	Uncorrected	Uncorrected
Center of mass correction	Uncorrected	Uncorrected
Tropospheric correction	IERS 2010 convention *(wet, wmf1, gpt2)*	IERS 2010 convention *(wet, wmf1, gpt2)*
Ionospheric correction	Second order ionospheric correction (Hernández-Pajares et al., 2007)	Second order ionospheric correction (Hernández-Pajares et al., 2007)
Elevation mask	15	15
Minimum visible satellite	4	4
Minimum satellite pass duration	300 s	350 s
Epochs deleted at each pass start	2 (20 sec)	2 (20 sec)
Minimum pass length for integer ambiguity computation	600 s	-
Kalman filter	Yes (more details about the algorithm in Barbu et al., 2018)	Yes (more details about the algorithm in Barbu et al., 2018)

---

[3] For more details about the GINS software, see GRGS, 2018; Marty et al., 2011. The reader may also refer to the paper of Kouba, 2015 for a description of the different parameters and models that can be used in the GNSS computation process.

Appendix D - Sea State Comparison between GNSS Buoy and 2019x pressure sensor

To be sure that the GNSS buoy and the 2019x pressure sensor monitor the same sea, we compare the Significant Wave Heights (SWH) from both instruments. As they are located 4km apart, we also used tide model predictions at both locations to compute a tidal gradient between both sensors.

SWH from the GNSS buoy

Located at the water surface, the GNSS buoy observations are directly impacted by the sea state, but also by longer variations such as tide or the geoid. To process theses data, we used the method describe in Bonnefond et al. (2003). To focus on the short variations, we differentiate between the filtered and the raw buoy data (RTKLib 1Hz differential solution). For that, GNSS heights are filtered using the Vondrak filter (Vondrak, 1977) with a cut-off period of 120s to remove short-wavelength oscillations (Figure D1a). Standard deviation of the residuals' heights (σ_{shr}) is compute using a 120s period's running average (Figure D1b). The standard deviation of the buoy due to waves (σ_{wave}) is then equal to: $\sigma_{wave} = \sqrt{\sigma_{shr}^2 - \sigma_{gps}^2}$ with σ_{gps} an estimation of the GNSS buoy processing errors (here estimate to be 2.5cm). The final Significant Wave Height (SWH) at the buoy is then derived from: $SWH = 4 \times \sigma_{wave}$ (Figure D1c).

SWH from the 2019x pressure sensors

The SBE26plus sensors have been set up to measure wave bursts during 10 minutes every hour (with 1 second wave sample duration). To compute the resulting SWH from theses wave bursts at 2019x, we first transform pressure records to equivalent hydrostatic depths atmospheric pressure time series from ERA5 (Hersbach et al., 2018) at the pressure gauge location, temperature from pressure recorder and a mean salinity of 35.5 psu. Then, we remove a linear trend for each burst of 512 values and reconstruct waves elevation. The Power Spectrum Density (PSD) is then estimated and the final waves parameters are extracted. After several tests, we choose a cut-off frequency of Fc=0.25 Hz. In order to easily compare with GNSS buoy SWH, this method is applied to the buoy observations, after selecting the same observation windows as from the pressure sensor's wave bursts.

SWH comparison

The results of the GNSS Buoy and 2019x pressure sensor SWH computation are showed in Figure D3a. We can see that the GNSS buoy, measuring at the direct water surface, is very sensitive to waves, down to frequency bands of 0.5Hz. If we apply the same cut-off frequency as the bottom pressure sensor (Fc=0.25) to the buoy data, we obtain a high correlation between the two series (c= 0.914, Figure D3b). Thus, at a depth of around 20 m, the pressure sensor is limited to a narrower frequency band than the buoy. But if we limit the comparison at the frequency band common to both systems, they roughly see the same sea.
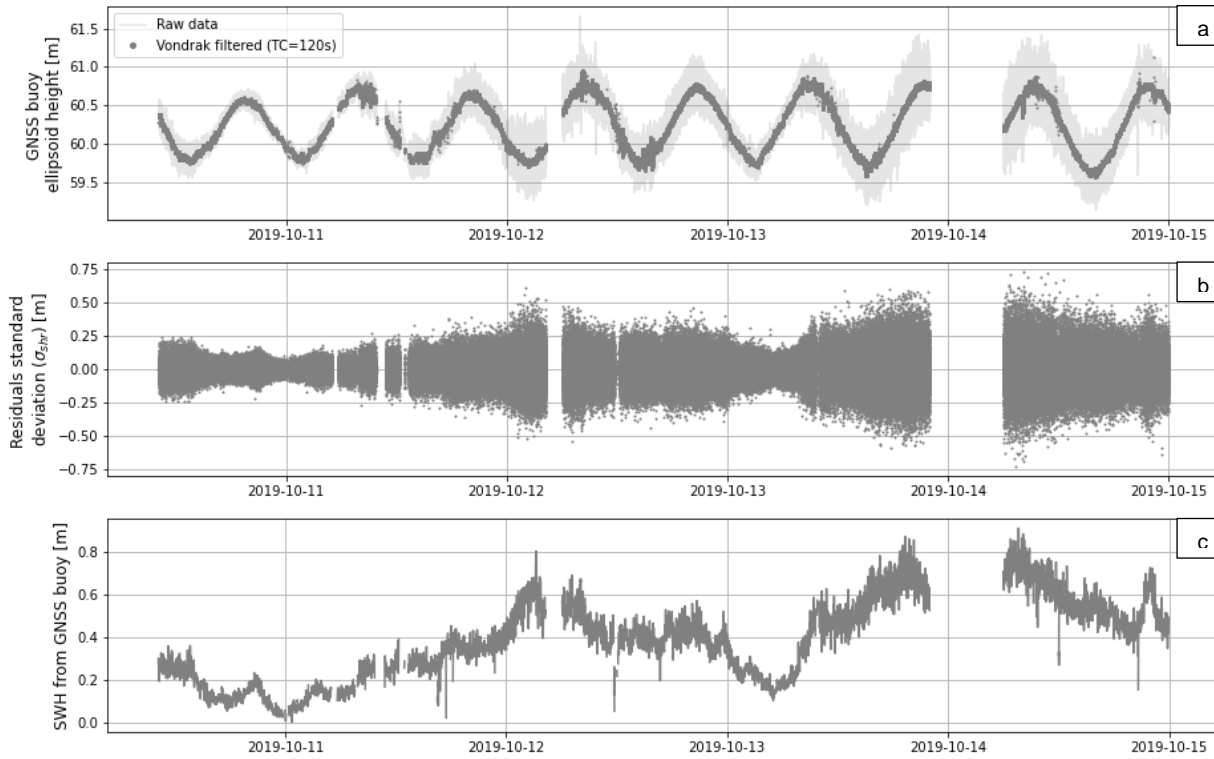
Figure D1. Computation step of the GNSS Buoy SWH / (a) Raw and Vondrak filtered GNSS buoy ellipsoid heights / (b) Standard deviation of the residuals' heights computed on 120s window (σ_{shr}) / (c) Significant Wave Height (SWH) at the buoy position.
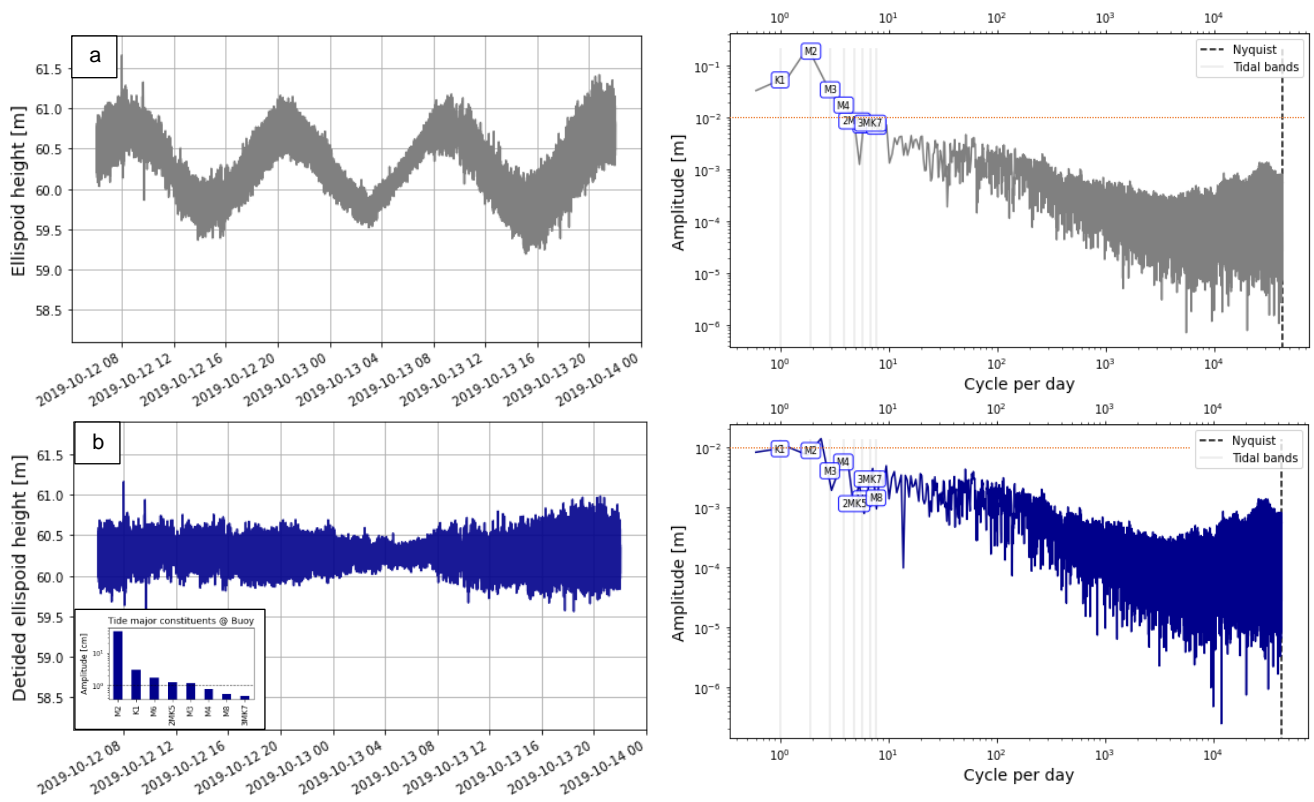
Figure D2. FFT computation for GNSS buoy observations of the 12th - 13th October 2019 / (a) GNSS buoy ellipsoid heights over the period
(left panel) and its corresponding FFT (right panel) / (b) GNSS buoy detided ellipsoid height (left panel) with the amplitude of the major
tide constituents at the buoy location and its corresponding FFT (right panel). Note that for the two FFT plot, the red dotted line highlights
the 10 cm amplitude.
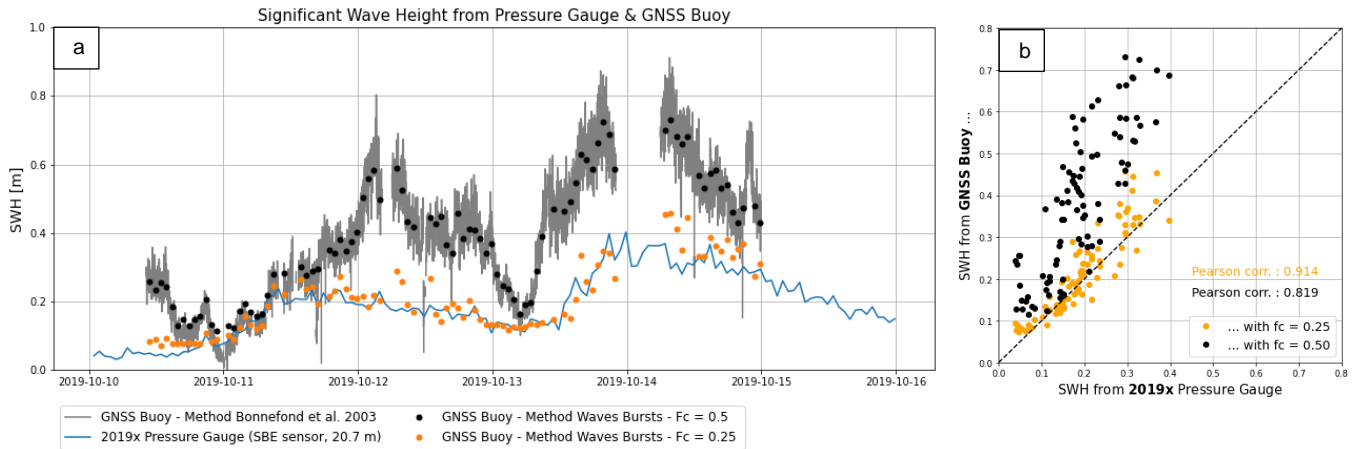
Figure D3. (a) Significant Wave Height from GNSS Buoy (grey line) and 2019x pressure gauge (blue line). To allow direct comparison,
the GNSS Buoy SWH is also compute with the wave burst method, using different cut-off frequencies (black and orange points). / (b)
Correlation between 2019x Pressure Gauge and GNSS Buoy SWH.

Tidal gradient between 2019x pressure gauge and buoy location

Although only 4km apart, the GNSS buoy and the pressure sensor may be subject to slightly different tidal regimes. We therefore used the output of the SCHISM hydrodynamic model, provided by Jérôme Lefevre from IRD in Noumea, to compute the tidal gradient between the two positions.

190

Figure D4 represents these results: the bar plots on the left panel shows the model extraction of amplitude and phase of the main tidal constituents at the buoy (blue) and pressure sensor location (orange). Differentiating the tide constituents [PG - Buoy], we obtain the amplitude and phase of the tidal gradient (red). The tide reconstruction due to this tidal gradient is showed in Figure D4c. We can see that over the 3 days of the GNSS buoy deployment, we could have height differences up to ± 1 cm

195   between the buoy and the pressure gauge location.
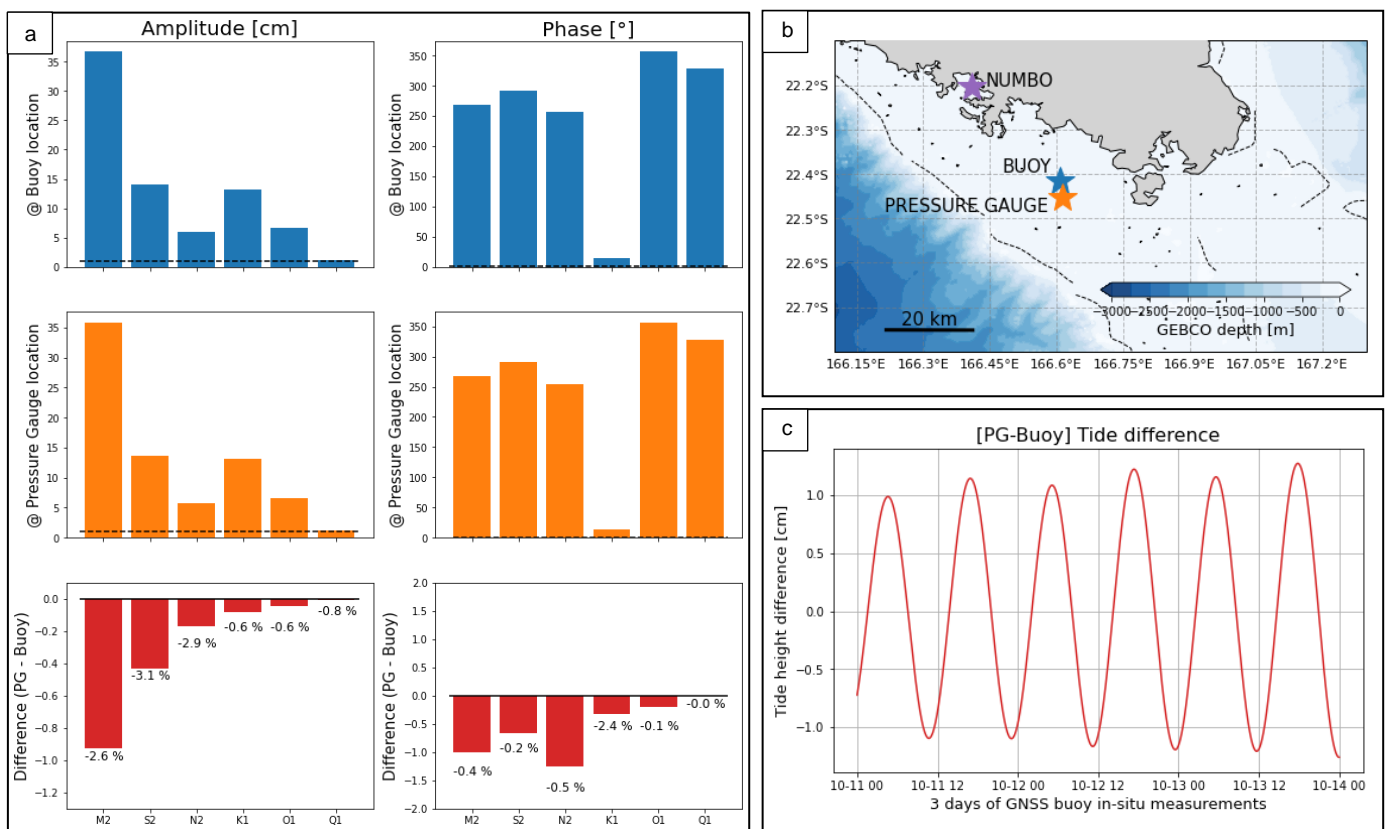
Figure D4. (a) Amplitude and phase of the six main tide constituents extracted from SCHISM hydrodynamic model at the buoy (blue) and pressure gauge location (orange). The red bar plot show amplitude and phase of the tide gradient between these two points. / (b) Location of the sensors. Note stars colours correspond to bar plot colours. / (c) Tide reconstruction over the 3 days of the GNSS buoy measurements

200   using amplitude and phase of the tide gradient.

These values are not negligible in our case, where we aim to get closer to the cm-level. Figure D5 represents the water heights difference observed by the GNSS buoy and the pressure sensor (see Section 3.3 for more details), considering or not this tidal
205 gradient. When comparing histograms of the residuals (Figure D5b), we can see that adding the gradient improves the distribution of the residuals, without impacting the mean bias. We have subsequently considered this tidal gradient to correct the observations of our pressure sensor.
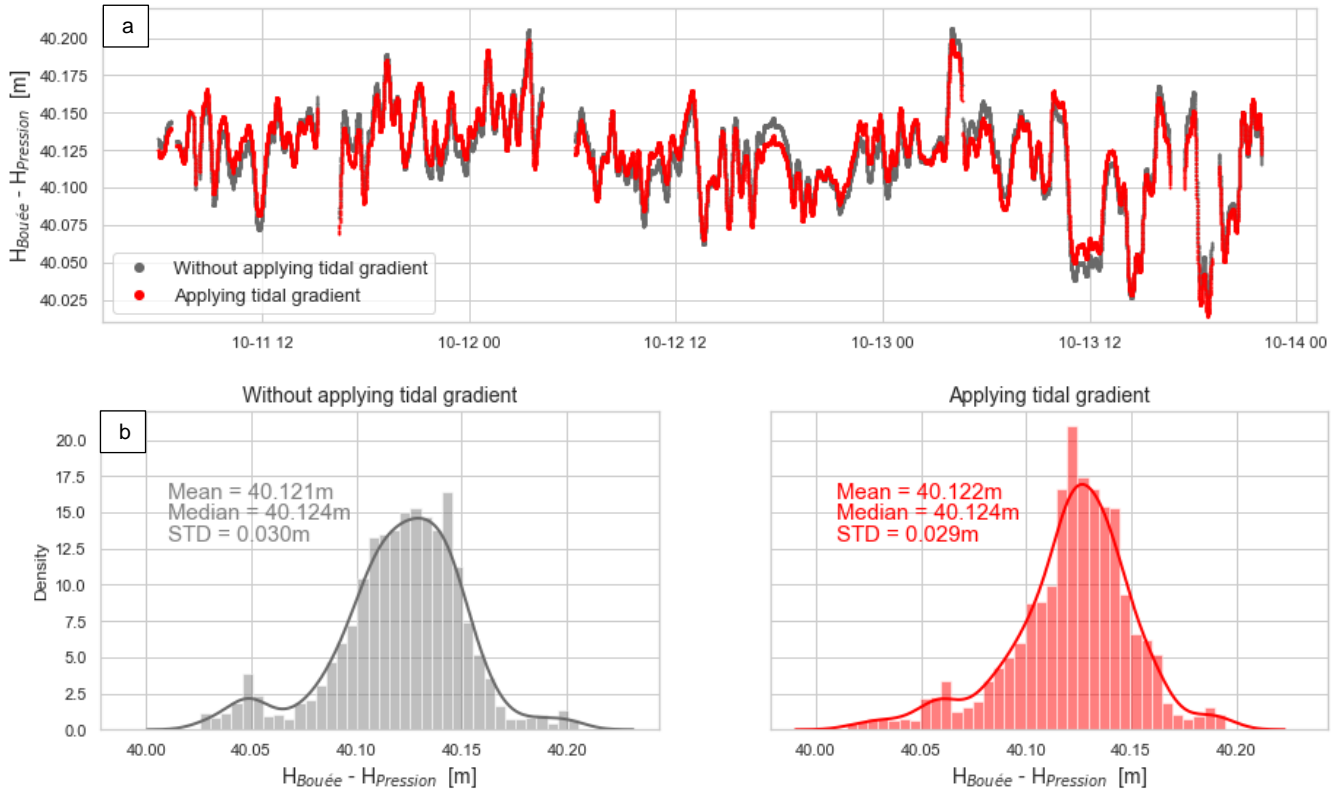
Figure D5. (a) Height difference over the 3 days of common observation period between the GNSS buoy and the pressure gauge (see
210 Section 3.3 for more details) considering (in red) or not (in grey) the tide gradient between the two locations. / (b) Histograms of the GNSS buoy and pressure gauge differences without (left panel – grey) or with (right panel – red) tide gradients.

Appendix E – Along-track altimetric wet tropospheric corrections

In the lagoon, the effect of coastal contamination on the radiometer data is visible when approaching the main island (Figure E1, grey area). However, the wet tropospheric correction seems to be exploitable at our comparison point for all missions (Figure E1, red area).
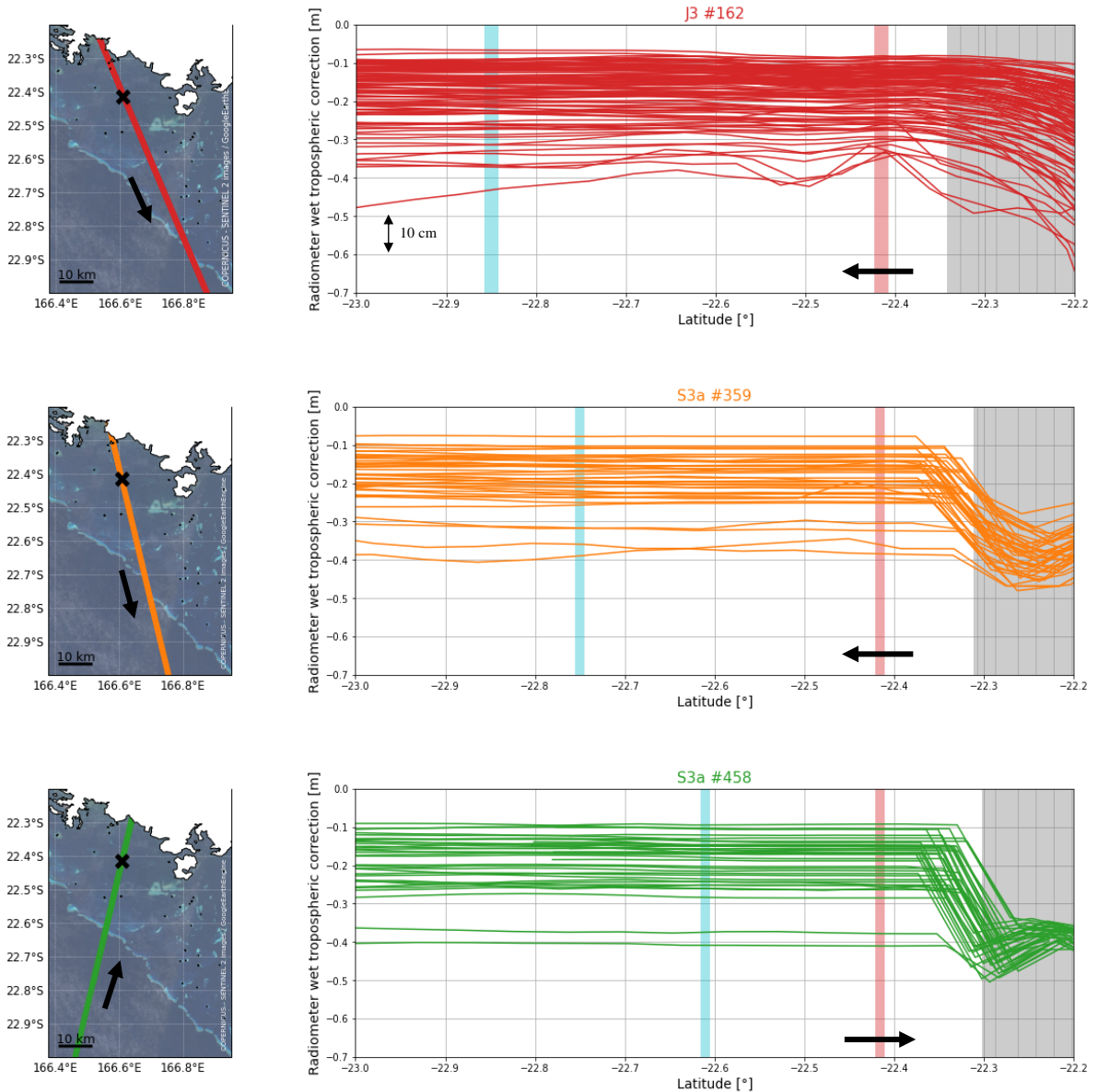
Figure E1. Evolution of the radiometer correction along the altimetric tracks used in our study (red for Jason 3 #162, orange for Sentinel-3a #359 and green for Sentinel-3a #458). The grey vertical bar represents the main island overfly, the red vertical bar represents the comparison point location and the blue vertical bar corresponds to the reef barrier overfly. Arrows symbolize the satellite direction of flight.
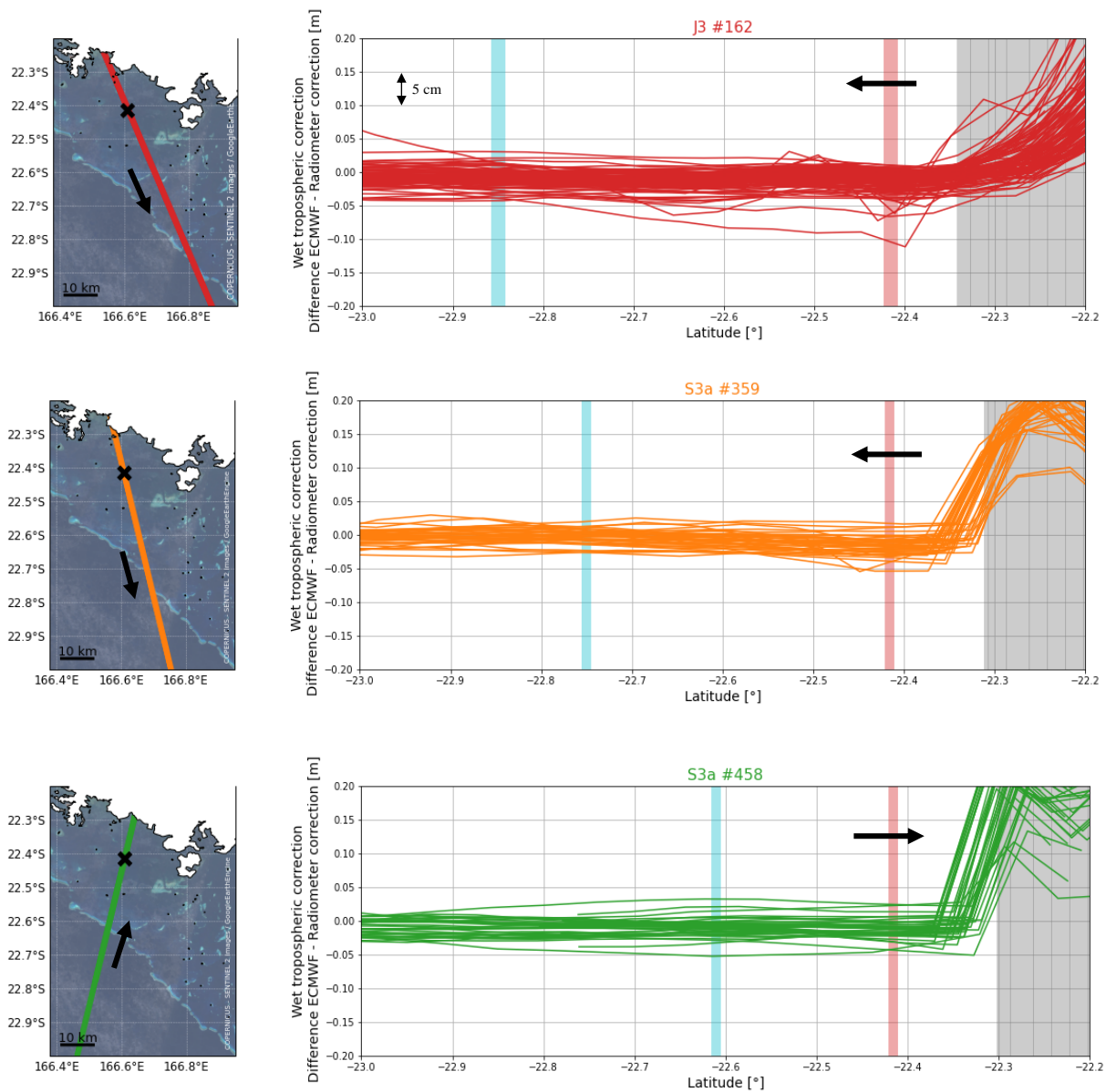
Figure E2. Evolution of the difference between ECMWF and the radiometer correction along the altimetric tracks used in our study (red for Jason 3 #162, orange for Sentinel-3a #359 and green for Sentinel-3a #458). The grey vertical bar represents the main island overfly, the red vertical bar represents the comparison point location and the blue vertical bar corresponds to the reef barrier overfly. Arrows symbolize the satellite direction of flight.

To test this hypothesis, we compared the correction provided by the radiometer with two data sets: (1) the wet tropospheric correction from the ECMWF model and (2) the wet tropospheric correction computed from permanent GNSS stations in Noumea. For the latter, we used the total tropospheric delay extracted from GINS PPP computations, performed by the CNES teams in Toulouse, for the NRMD and NOUM stations. The tropospheric corrections, estimated every 2 hours, are interpolated at the satellite pass times. The dry tropospheric component from GDR files is then subtracted to finally obtain the wet component of the tropospheric correction. Since the GNSS stations are not at sea level elevation, an additional correction is applied to account for the pressure difference with the comparison point (which is at sea level elevation). For this, we used the Saastamoinen equations (Saastamoinen, 1972) according to the method described by Kouba (2008).

To illustrate the objective of our comparison, we represent the wet tropospheric delay from radiometer, ECMWF model and GNSS data along the Jason 3 track #162 for 3 random cycles (Figure E3). If we focus on our study area (the grey area on Figure E3), we can see that the three solutions can be very variable according to the cycles and can affect the estimate of the altimetric SSH at the centimetric level.
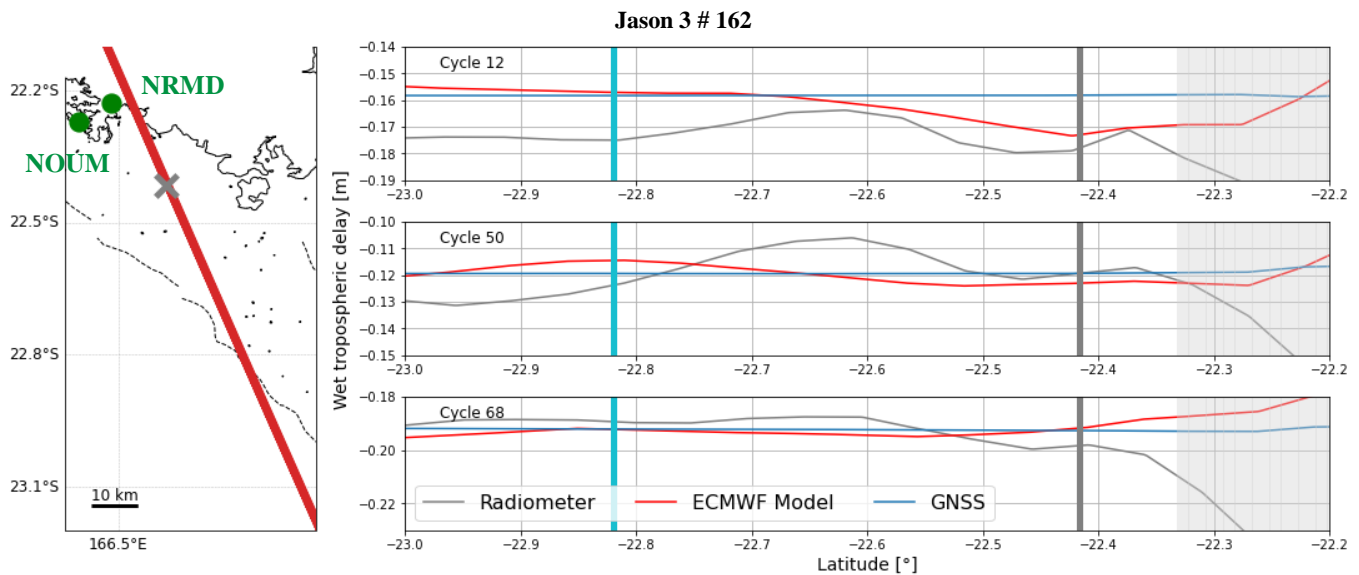
Figure E3. Wet tropospheric correction from radiometer (grey), ECMWF model (red) and GNSS stations (blue) for three random cycles of the Jason 3 #162. On the right panel, the light grey area represents the main island overfly, the dark grey area represents the comparison point overfly and the blue area corresponds to the reef barrier overfly.

Appendix F - Validation of gradients from global geoïd models in the lagoon

Another objective of the cruise was to improve sea level kinematic mapping methodology in coastal areas through the deployment and comparison of multiple sensors, as described in Chupin et al. 2020. For that purpose, the coastal version of the CalNaGeo GNSS carpet was towed by R/V ALIS along and across altimetry tracks, and inside and outside the lagoon (Figure 1b, blue lines). The 10s observations of CalNaGeo were processed with GINS in PPP mode (Marty et al., 2011) (processing details in Appendix C), and filtered using the Vondrak filter with a cutoff period of 30 min (~ 5.4 km at 6 knots). The 2019x pressure sensor is then used to remove the time-varying component of CalNaGeo measurements (especially the oceanic tide, assuming that it does not vary spatially over our area). Thanks to these data, we then analyse the performance of different models to estimate geoid gradients.

Three datasets were selected to conduct our comparison:

- The XGM2019e global gravity field model (Zingerle et al., 2020), represented by spherical harmonics corresponding to a spatial resolution of 2' (~4 km). This model is based on GOCO06s satellite data combined with terrestrial measurements for shorter wavelengths. Gravity anomalies derived from satellite altimetry are used over oceans (DTU13).
- The global Earth gravity potential model EGM2008 (Pavlis et al., 2012) defined on a 5' arc (~10 km) equiangular grid. This model is based on terrestrial, altimetric and airborne gravity data.
- An average model of the Earth's gravity field, the EIGEN-GRGS.RL04.MEAN-FIELD (Lemoine et al., 2019), hereafter referred as EIGEN, computed from the RL04 GRACE+SLR monthly time series and GOCE data.

Along CalNaGeo track, the comparison with XGM2019e and EGM08 gradients shows no significant differences (resp. Fig. F1b and F1c). On the contrary, the comparison with the EIGEN model shows a residual southeast/northwest gradient of about 1.8 cm/km (Figure F1d). In our process, we thus select the XGM2019e model to account for geoid gradients. This first study allowed us to select the most relevant model for our area, but further analysis is still required to refine the CalNaGeo GNSS solution and to map the mean sea surface over the whole lagoon.

Table F1. Geoïd height difference between 2019x pressure gauge (4 km south of the crossover) and Noumea tide-gauge site

	Geoïd height difference	
XGM 2019e (Zingerle et al., 2020)	-52.4 cm	
EGM 2008 (Pavlis et al., 2012)	- 54.9 cm	
EIGEN (Lemoine et al., 2019)	- 27.0 cm	
Our study ($\Delta datum_{TG \to PG}$)	- 57.1 cm	
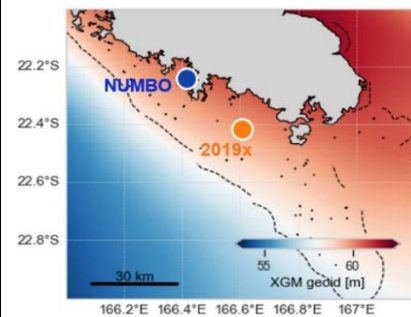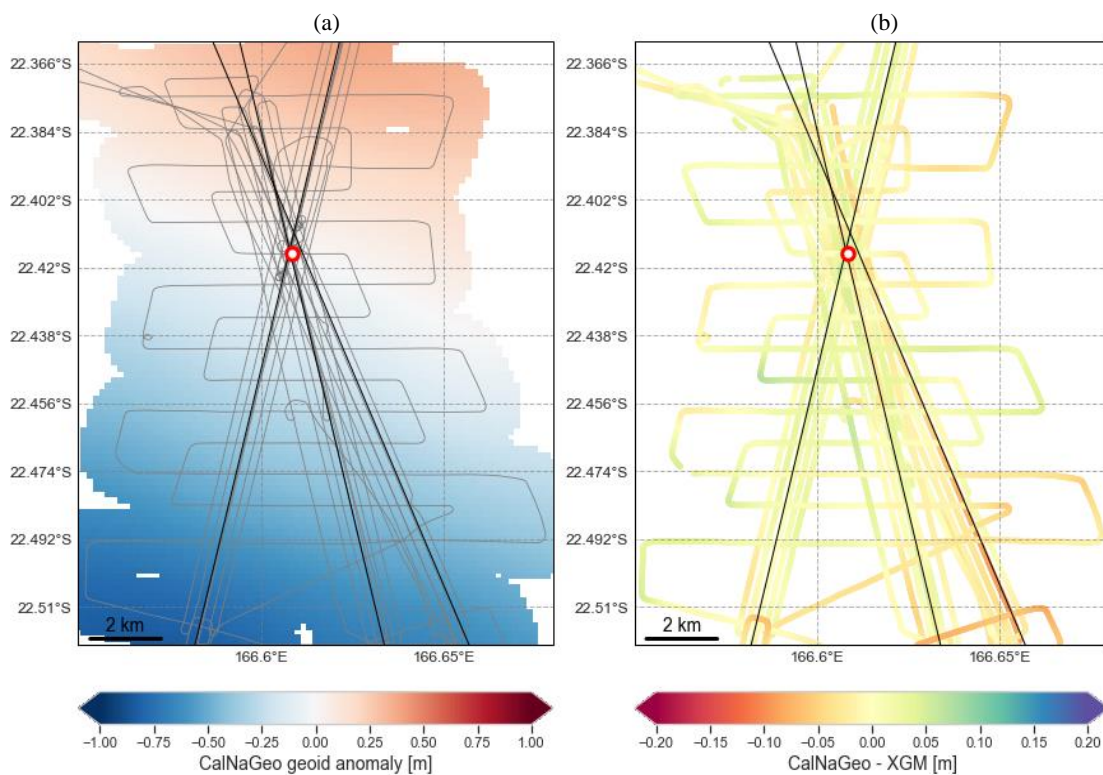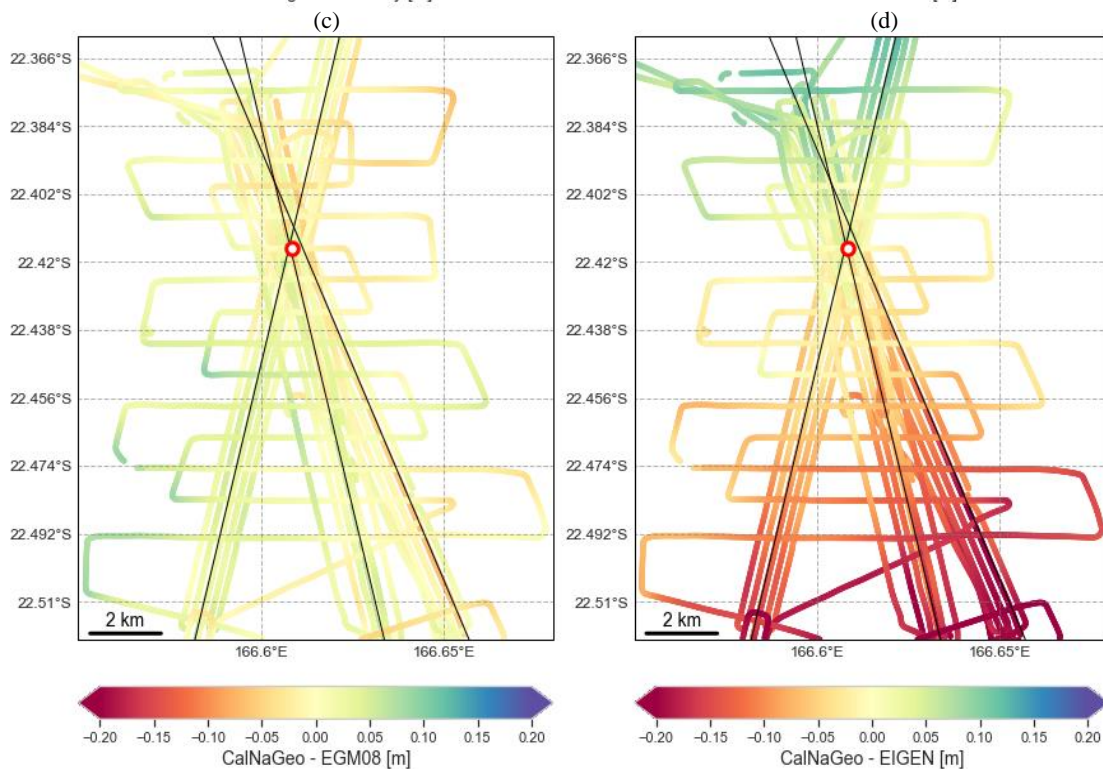
Figure F1. Comparison of global gravity field models with CalNaGeo measurements. / (a) Mean sea surface anomalies from CalNaGeo measurements during the GEOCEAN-NC cruise, expressed with respect to the altimeter comparison point (red dot on the map) / (b) Difference between CalNaGeo and the XGM2019e model with respect to the comparison point. / (c) Difference between CalNaGeo and the EGM08 model with respect to the comparison point. / (d) Difference between CalNaGeo and the EIGEN model with respect to the comparison point.

Appendix G – Assessment of altimetry data quality in the lagoon

The retracking provides the range by fitting a theorical model on the radar echo recorded by the altimeter. The Mean Quadratic Error (MQE) parameter give an idea of the retracking process: the closer the MQE is to zero, the better the chosen model reproduce the measured waveform. So far, altimetry products do not give any indication of a valid on invalid MQE value. To get an idea of the "threshold" value of the MQE parameter that could discriminate valid or invalid ocean waveforms, we conducted an analysis on two Jason 3 and two Sentinel-3a tracks. For all cycles between 2016 and 2019, we extract along track 20Hz MQE parameter and compare them to the coastline distance.
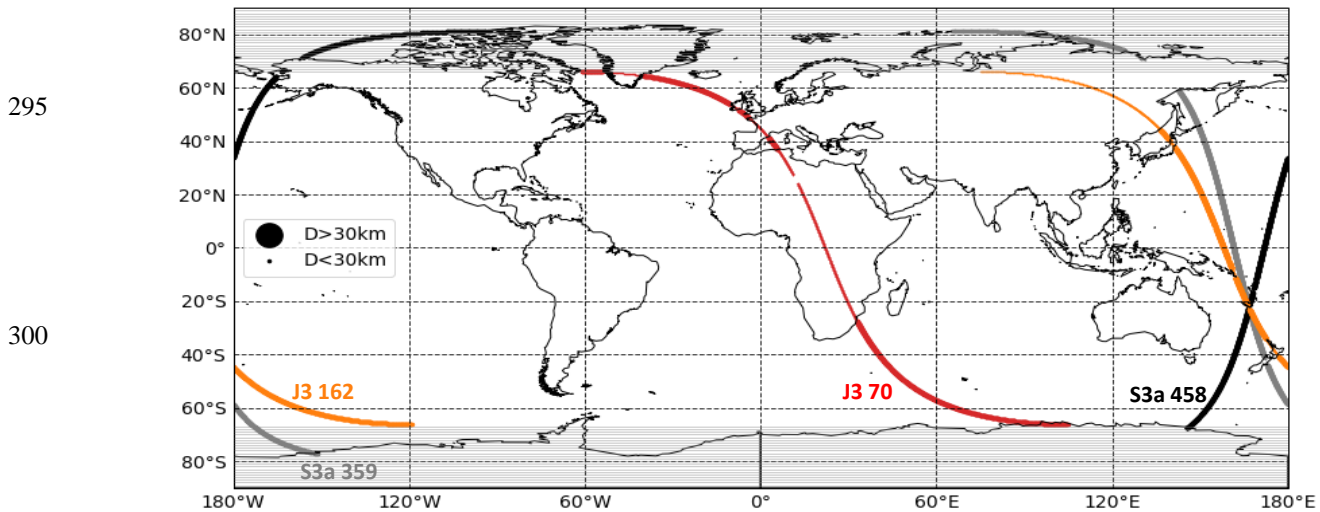
Figure G1. Distance to nearest coastline from the along-track point of the 2 Jason and 2 Sentinel tracks used to analyse the MQE parameter. The big dots represent along-track points distant from more than 30km to the nearest coastline, and the small dots are point located on lands or less than 30km to the coastline. Note that to have a consistent comparison between both missions, Sentinel points located in polar areas (between -90°/-66° and 90°/66°) are not considered in the computation.
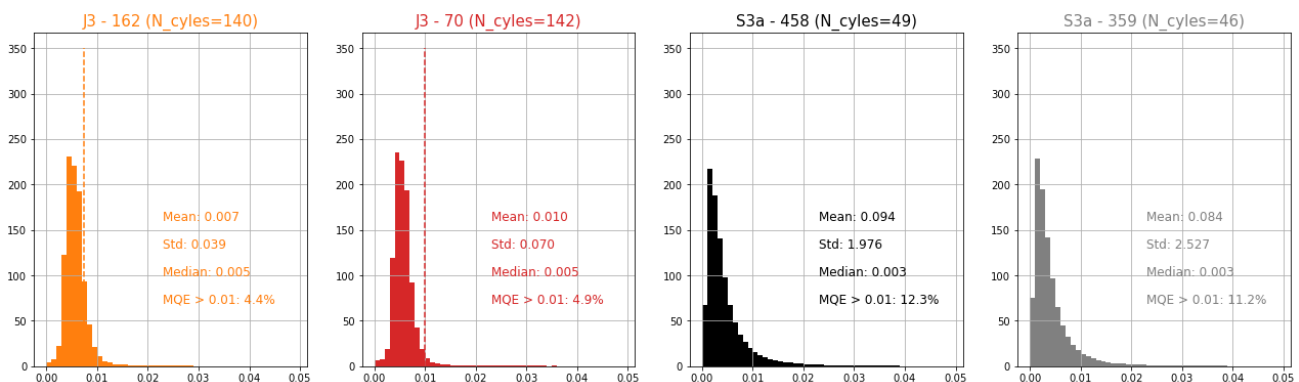
Figure G2. Statistics on the MQE values of points located more than 30km from the coast (considered as oceanic points). The dashed line represents the mean value.
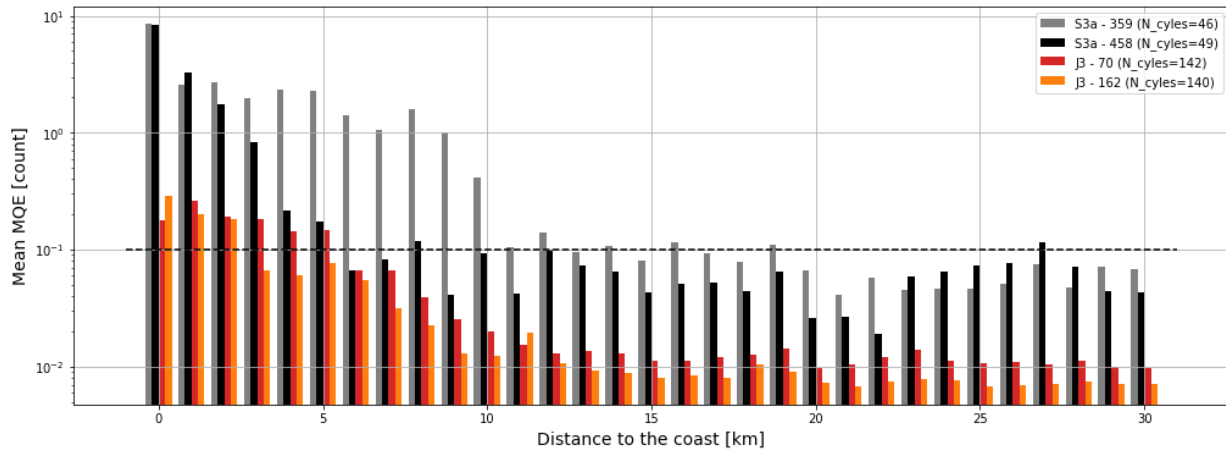
Figure G3. Mean values of MQE parameter function of the distance to the coast.

310   For Jason 3, our analysis shows that in the open ocean (*i.e.* distance to the coast > 30 km), the mean MQE parameter is less than or equal to 0.01 (Figure G2, red and orange). Along the Sentinel-3a tracks, this mean MQE value is more variable with a standard deviation of 2/2.5 (compared to 0.04/0.07 for Jason). However, the median is well below 0.01, suggesting that extreme values influence the estimate of the mean (Figure G2, grey and black). Approaching the coast, the MQE parameter increases significantly (Figure G3). In the 10/15 km range, the mean MQE tends towards 0.01 for Jason, but tends 0.1 for

315   Sentinel (Figure G3). We could therefore consider that MQE values greater than 0.01 could indicate an improper retracking and therefore potentially erroneous water depths. These preliminary results are strongly influenced by the tracks geometry, and a global analysis of all satellite passes would help to determine a more realistic threshold value for each mission.

       However, to analyse our dataset, we considered that a MQE value above 0,01 may indicate a non-oceanic radar signal for

320   both Jason and Sentinel missions. Figure G4 shows the 20Hz along-track MQE parameter for the three tracks over the year 2019. There is about 3 times more Jason than Sentinel data, because of the difference in revisit period (respectively 9.9 and 27 days for Jason 3 and Sentinel satellites). We can note that for each track, the MQE parameter is higher and more variable at the coral reef overfly (black dotted line). Closer to the coast, the MQE parameter in the crossover area (black box) is mostly below 0.01, indicating that the waveforms retracking using the open ocean model is suitable for most passes. As the retracking

325   allows to determine the altimeter range, and thus to compute the altimeter Sea Surface Height, this result supports the idea that SSH altimetry data in our comparison area are reliable.
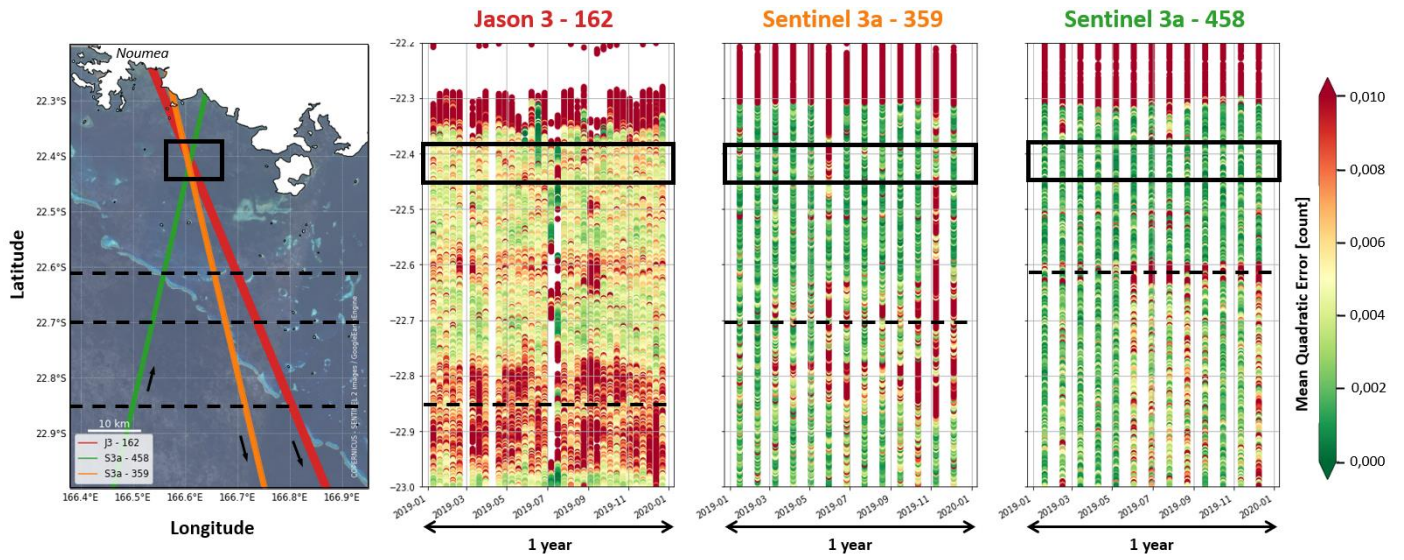
330 **Figure G4.** Along track Mean Quadratic Error (MQE) parameter for the 3 satellites passes that crosses in the lagoon during year 2019. The grey area represents the crossing area, and the black dotted lines the open-ocean/lagoon interface for each track.

References

335   Aucan, J., Merrifield, M. A., and Pouvreau, N.: Historical Sea Level in the South Pacific from Rescued Archives, Geodetic Measurements, and Satellite Altimetry, Pure Appl. Geophys., 174, 3813–3823, https://doi.org/10.1007/s00024-017-1648-1, 2017a.

Aucan, J., Vendé-Leclerc, M., Dumas, P., and Bricquir, M.: Wave forcing and morphological changes of New Caledonia lagoon islets: Insights on their possible relations, Comptes Rendus Geosci., 349, 248–259,
340   https://doi.org/10.1016/j.crte.2017.09.003, 2017b.

Ballu, V., Gravelle, M., Woppelmann, G., de Viron, O., Rebischung, P., Becker, M., and Sakic, P.: Vertical land motion in the Southwest and Central Pacific from available GNSS solutions and implications for relative sea levels, Geophys. J. Int., 218, 1537–1551, https://doi.org/10.1093/gji/ggz247, 2019.

Barbu, A. L., Laurent-Varin, J., Perosanz, F., Mercier, F., and Marty, J.-C.: Efficient QR sequential least square algorithm for
345   high frequency GNSS precise point positioning seismic application, Adv. Space Res., 61, 448–456, https://doi.org/10.1016/j.asr.2017.10.032, 2018.

Becker, M., Meyssignac, B., Letetrel, C., Llovel, W., Cazenave, A., and Delcroix, T.: Sea level variations at tropical Pacific islands since 1950, Glob. Planet. Change, 80–81, 85–98, https://doi.org/10.1016/j.gloplacha.2011.09.004, 2012.

Blewitt, G., Kreemer, C., Hammond, W. C., and Gazeaux, J.: MIDAS robust trend estimator for accurate GPS station velocities
350   without step detection, J. Geophys. Res. Solid Earth, 121, 2054–2068, https://doi.org/10.1002/2015JB012552, 2016.

Bonnefond, P., Exertier, P., Laurain, O., Ménard, Y., Orsoni, A., Jeansou, E., Haines, B. J., Kubitschek, D. G., and Born, G.: Leveling the Sea Surface Using a GPS-Catamaran, Mar. Geod., 26, 319–334, https://doi.org/10.1080/714044524, 2003.

Bonneton, P., Lefebvre, J.-P., Bretel, P., Ouillon, S., and Douillet, P.: Tidal modulation of wave-setup and wave-induced currents on the Aboré coral reef, New Caledonia, J. Coast. Res., 762–766, 2007.

355   Chupin, C., Ballu, V., Testut, L., Tranchant, Y.-T., Calzas, M., Poirier, E., Coulombier, T., Laurain, O., Bonnefond, P., and Team FOAM Project: Mapping Sea Surface Height Using New Concepts of Kinematic GNSS Instruments, Remote Sens., 12, 2656, https://doi.org/10.3390/rs12162656, 2020.

DeMets, C., Gordon, R. G., and Argus, D. F.: Geologically current plate motions, Geophys. J. Int., 181, 1–80, https://doi.org/10.1111/j.1365-246X.2009.04491.x, 2010.

360   Douillet, P.: Tidal dynamics of the south-west lagoon of New Caledonia: observations and 2D numerical modelling, Oceanol. Acta, 21, 69–79, https://doi.org/10.1016/S0399-1784(98)80050-9, 1998.

Garcin, M., Vendé-Leclerc, M., Maurizot, P., Le Cozannet, G., Robineau, B., and Nicolae-Lerma, A.: Lagoon islets as indicators of recent environmental changes in the South Pacific – The New Caledonian example, Cont. Shelf Res., 122, 120–140, https://doi.org/10.1016/j.csr.2016.03.025, 2016.

365   Gravelle, M., Wöppelmann, G., Gobron, K., Altamimi, Z., Guichard, M., Herring, T., and Rebischung, P.: The ULR-repro3 GPS data reanalysis and its estimates of vertical land motion at tide gauges for sea level science, Earth Syst. Sci. Data Discuss., 2022, 1–22, https://doi.org/10.5194/essd-2022-235, 2022.

GRGS: Algorithmic documentation of the GINS software, 2018.

Hammond, W. C., Blewitt, G., Kreemer, C., and Nerem, R. S.: GPS Imaging of Global Vertical Land Motion for Studies of Sea Level Rise, J. Geophys. Res. Solid Earth, 126, https://doi.org/10.1029/2021JB022355, 2021.

Heflin, M., Donnellan, A., Parker, J., Lyzenga, G., Moore, A., Ludwig, L. G., Rundle, J., Wang, J., and Pierce, M.: Automated Estimation and Tools to Extract Positions, Velocities, Breaks, and Seasonal Terms From Daily GNSS Measurements: Illuminating Nonlinear Salton Trough Deformation, Earth Space Sci., 7, e2019EA000644, https://doi.org/10.1029/2019EA000644, 2020.

Hernández-Pajares, M., Juan, J. M., Sanz, J., and Orús, R.: Second-order ionospheric term in GPS: Implementation and impact on geodetic estimates, J. Geophys. Res. Solid Earth, 112, https://doi.org/10.1029/2006JB004707, 2007.

Hersbach, H., Bell, B., Berrisford, P., Biavati, G., Horányi, A., Muñoz Sabater, J., Nicolas, J., Peubey, C., Radu, R., Rozum, I., Schepers, D., Simmons, A., Soci, C., Dee, D., and Thépaut, J.-N.: ERA5 hourly data on pressure levels from 1979 to present, Copernicus Climate Change Service (C3S) Climate Data Store (CDS), 2018.

Jouon, A., Lefebvre, J. P., Douillet, P., Ouillon, S., and Schmied, L.: Wind wave measurements and modelling in a fetch-limited semi-enclosed lagoon, Coast. Eng., 56, 599–608, https://doi.org/10.1016/j.coastaleng.2008.12.005, 2009.

Jullien, S., Aucan, J., Lefèvre, J., Peltier, A., and Menkes, C. E.: Tropical Cyclone Induced Wave Setup around New Caledonia during Cyclone COOK (2017), J. Coast. Res., 95, 1454, https://doi.org/10.2112/SI95-281.1, 2020.

Kouba, J.: Implementation and testing of the gridded Vienna Mapping Function 1 (VMF1), J. Geod., 82, 193–205, https://doi.org/10.1007/s00190-007-0170-0, 2008.

Lemoine, J.-M., Biancale, R., Reinquin, F., Bourgogne, S., and Gégout, P.: CNES/GRGS RL04 Earth gravity field models, from GRACE and SLR data, 2019.

Männel, B., Schöne, T., Bradke, M., and Schuh, H.: Vertical Land Motion at Tide Gauges Observed by GNSS: A New GFZ-TIGA Solution, Springer Berlin Heidelberg, Berlin, Heidelberg, 1–9, https://doi.org/10.1007/1345_2022_150, 2022.

Martínez-Asensio, A., Wöppelmann, G., Ballu, V., Becker, M., Testut, L., Magnan, A. K., and Duvat, V. K. E.: Relative sea-level rise and the influence of vertical land motion at Tropical Pacific Islands, Glob. Planet. Change, 176, 132–143, https://doi.org/10.1016/j.gloplacha.2019.03.008, 2019.

Marty, J. C., Loyer, S., Perosanz, F., Mercier, F., Bracher, G., Legresy, B., Portier, L., Capdeville, H., Fund, F., Lemoine, J. M., and Biancale, R.: GINS: The CNES/GRGS GNSS scientific software, in: ESA Proceedings WPP326, 3 rd International Colloquium Scientific and Fundamental Aspects of the Galileo Programme, Copenhagen, Denmark, 2011.

Nerem, R. S. and Mitchum, G. T.: Estimates of vertical crustal motion derived from differences of TOPEX/POSEIDON and tide gauge sea level measurements, Geophys. Res. Lett., 29, 40-1-40–4, https://doi.org/10.1029/2002GL015037, 2002.

Okada, Y.: Surface deformation due to shear and tensile faults in a half-space, Bull. Seismol. Soc. Am., 75, 1135–1154, https://doi.org/10.1785/BSSA0750041135, 1985.

Pavlis, N. K., Holmes, S. A., Kenyon, S. C., and Factor, J. K.: The development and evaluation of the Earth Gravitational Model 2008 (EGM2008), J. Geophys. Res. Solid Earth, 117, https://doi.org/10.1029/2011JB008916, 2012.

Peltier, W. R., Argus, D. F., and Drummond, R.: Space geodesy constrains ice age terminal deglaciation: The global ICE-6G_C (VM5a) model, J. Geophys. Res. Solid Earth, 120, 450–487, https://doi.org/10.1002/2014JB011176, 2015.

Saastamoinen, J.: Atmospheric Correction for the Troposphere and Stratosphere in Radio Ranging Satellites, in: Geophysical Monograph Series, edited by: Henriksen, S. W., Mancini, A., and Chovitz, B. H., American Geophysical Union, Washington, D. C., 247–251, https://doi.org/10.1029/GM015p0247, 1972.

Vondrak, J.: Problem of Smoothing Observational Data II, Astron. Institue Czechoslov. Acad. Sci. Praha, 28, 84–89, 1977.

Weatherall, P., Marks, K. M., Jakobsson, M., Schmitt, T., Tani, S., Arndt, J. E., Rovere, M., Chayes, D., Ferrini, V., and Wigley, R.: A new digital bathymetric model of the world's oceans, Earth Space Sci., 2, 331–345, https://doi.org/10.1002/2015EA000107, 2015.

Zingerle, P., Pail, R., Gruber, T., and Oikonomidou, X.: The combined global gravity field model XGM2019e, J. Geod., 94, 66, https://doi.org/10.1007/s00190-020-01398-0, 2020.